

ORTHOGONAL MULTI-VIEW ANALYSIS BY SUCCESSIVE APPROXIMATIONS VIA EIGENVECTORS

LI WANG, LEI-HONG ZHANG, CHUNGEN SHEN, AND REN-CANG LI

ABSTRACT. We propose a unified framework for multi-view subspace learning to learn individual orthogonal projections for all views. The framework integrates the correlations within multiple views, supervised discriminant capacity, and distance preservation in a concise and compact way. It not only includes several existing models as special cases, but also inspires new novel models. To demonstrate its versatility to handle different learning scenarios, we showcase three new multi-view discriminant analysis models and two new multi-view multi-label classification ones under this framework. An efficient numerical method based on successive approximations via eigenvectors is presented to solve the associated optimization problem. The method is built upon an iterative Krylov subspace method which can easily scale up for high-dimensional datasets. Extensive experiments are conducted on various real-world datasets for multi-view discriminant analysis and multi-view multi-label classification. The experimental results demonstrate that the proposed models are consistently competitive to and often better than the compared methods that do not learn orthogonal projections.

1. INTRODUCTION

Multi-view data are increasingly collected for a variety of applications in the real world. They usually contain complementary, redundant, and corroborative contents and so are more informative than single-view data when it comes to characterize objects of the real-world. It is rather natural for human beings to perceive the world through comprehensive information collected by multiple sensory organs, but it is an open question on how to endow machines with analogous cognitive capabilities to do the same. One of the fundamental challenges is how to represent and summarize multi-view data in such a way that comprehensive information concealed in multi-view data can be properly exploited by multi-view learning models.

The heterogeneity gap [1] among multiple views makes it challenging to construct such representations since features extracted from different views with similar semantics may be located in completely different subspaces, e.g., text is often symbolic while audio and image are signals. A significant research effort has been

Li Wang is with Department of Mathematics and Department of Computer Science and Engineering, University of Texas at Arlington, Arlington, TX 76019-0408, USA. Email: li.wang@uta.edu. Corresponding Author.

Lei-Hong Zhang is with School of Mathematical Sciences and Institute of Computational Science, Soochow University, Suzhou 215006, Jiangsu, China. Email: longzlh@suda.edu.cn.

Chungen Shen is with College of Science, University of Shanghai for Science and Technology, Shanghai 200093, China. Email: shenchungen@usst.edu.cn.

Ren-Cang Li is with Department of Mathematics, University of Texas at Arlington, Arlington, TX 76019-0408, USA. Email: rcli@uta.edu.

about narrowing this gap by seeking a common semantic subspace into which the heterogeneous features from different views are projected.

Multi-view subspace learning, as the most popularly studied methodology for multi-view learning [2, 3], aims to narrow the heterogeneity gap under the assumption that all views are generated from a common latent space via some unknown transformations in the first place. The most representative subspace learning model is the canonical correlation analysis (CCA) [4], which was originally proposed to learn two linear projections by maximizing the cross-correlation between two views in a common space. It has since been extended to more than two views [5], nonlinear projections via either kernel representation [6] or deep representation [7], supervised learning [8, 9, 10], and multi-output learning such as multi-label classification [11] and multi-target regression [12].

Recent researches have demonstrated that orthogonality built into single-view subspace learning models admits desirable advantages such as more noise-tolerant, better suited for data visualization and distance preservation [13, 14, 15, 16, 17, 18]. An orthogonal projection preserves the pairwise distance so long as the vectors to be projected live in the range of the projection. Distance preservation, as one of the most important learning criteria, has also been successfully demonstrated in learning methods such as kernel learning [19] and density estimation [20].

Orthogonality has been successfully explored in multi-view subspace learning, including orthogonal CCA (OCCA) [12, 21, 22, 23], orthogonal multiset CCA (OMCCA) [23, 24], and multi-view partial least squares (PLS) [25]. However, most multi-view subspace learning methods stay clear from orthogonality constraints for two technical obstacles:

- 1) adding orthogonality constraints may cause incompatibility to inherent constraints already there in existing models, and
- 2) even if there is no incompatibility issue, the resulting optimization problem is generally hard to solve.

Generic optimization methods are often too slow even for datasets of modest scale and practically infeasible for high dimensional data. As a result, most existing learning methods [8, 9, 26] resort to solving certain related relaxed problems of their original formulations as generalized eigenvalue problems, for which well-developed numerical linear algebra techniques can be readily deployed to handle high-dimensional datasets but at a price of degrading learning performance.

This issue has been previously studied in the case of the trace ratio formulation *vs.* the ratio trace formulation for single-view dimensionality reduction in the context of linear discriminant analysis (LDA). Authors in [15] argued that the trace ratio formulation with the orthogonality constraint is essential and can lead to superiority over the ratio trace formulation which is a relaxation of the trace ratio formulation as a generalized eigenvalue problem. The cross-correlation between two views in CCA is inherently defined as a trace ratio formulation [4]. Moreover, the objective function of the trace ratio formulation is invariant under any orthogonal transformation, which is more beneficial to classification and clustering in the reduced space than the ratio trace formulation that is invariant under any non-singular transformation. This motivates the study of orthogonal LDA (OLDA) [15, 16] and orthogonal CCA (OCCA) [22]. However, no orthogonal extension to supervised multi-view subspace learning has yet been explored.

Our goals in this paper are twofold. We will propose a unified framework for orthogonal multi-view analysis to resolve the obstacle 1) we previously pointed out. Specifically, we take the trace ratio formulation to model the pairwise correlations of multiple views by strictly following their original definitions. Various supervised information can be incorporated into the numerators or denominators of the trace ratios in order to capture the class separability or coherence. Orthogonality constraints are added without causing any incompatibility issue. All three ingredients are integrated together in a concise and consistent way by the proposed framework. However, the resulting optimization problem is a challenging one. That is the obstacle 2) we previously pointed out. Instead of solving the optimization problem as it is, we propose an efficient optimization method called orthogonal successive approximation via eigenvectors (OSAVE) to calculate an approximate solution.

Contributions. The main contributions of this paper are summarized as follows:

- We propose a unified multi-view subspace learning framework, which can naturally integrate the dependency among multiple views, supervised information, and simultaneously learn orthogonal projections in a concise and compact formulation. OLDA, OCCA and OMCCA are special cases of the proposed framework.
- Our framework can be flexibly adapted for various learning scenarios. To justify the flexibility, we instantiate several new models from the proposed framework. Three models are proposed for multi-view feature extraction, and two models for multi-view multi-label classification. Different from existing ones, our models are directly built on the essential trace ratio formulation with orthogonality constraints.
- To solve the challenging optimization problem of the proposed framework, we present a successive approximation algorithm, which is built upon well-developed numerical linear algebra techniques. We describe an iterative Krylov subspace method for calculating the top eigenvector of generalized eigenvalue problem $A\mathbf{x} = \lambda B\mathbf{x}$ with possibly a singular B . The Krylov subspace method can serve as the workhorse for scalability.
- Extensive experiments are conducted for evaluating the proposed models against existing learning methods in terms of two learning tasks: multi-view feature extraction and multi-view multi-label classification. Experimental results on various real-world datasets demonstrate that our proposed models perform competitively to and often better than baselines.

Paper organization. We first describe the background of this work from single- and multi-view feature extraction and briefly review the relevant existing models in Section 2. In Section 3, we propose the novel unified framework for orthogonal multi-view analysis, and their instantiated models for multi-view discriminant analysis and multi-view multi-label classification. The proposed successive approximation algorithm is presented in Section 5 with its key component in Section 4. Extensive experiments are conducted in Section 6. Finally, we draw our conclusions in Section 7.

Notation. $\mathbb{R}^{m \times n}$ is the set of $m \times n$ real matrices and $\mathbb{R}^n = \mathbb{R}^{n \times 1}$. $I_n \in \mathbb{R}^{n \times n}$ is the identity matrix of size $n \times n$, and $\mathbf{1}_n \in \mathbb{R}^n$ is the vector of all ones. $\|\mathbf{x}\|_2$ is the 2-norm of a vector $\mathbf{x} \in \mathbb{R}^n$. For $B \in \mathbb{R}^{m \times n}$, $\mathcal{R}(B)$ is the column subspace. $B \succ 0$ ($\succeq 0$) means that B is symmetric positive definite (semi-definite). The Stiefel

manifold

$$(1) \quad \mathbb{O}^{n \times k} = \{X \in \mathbb{R}^{n \times k} : X^T X = I_k\}$$

is an embedded submanifold of $\mathbb{R}^{n \times k}$ endowed with the standard inner product $\langle X, Y \rangle = \text{tr}(X^T Y)$ for $X, Y \in \mathbb{R}^{n \times k}$, where $\text{tr}(X^T Y)$ is the trace of $X^T Y$.

2. BACKGROUND AND RELATED WORK

Feature extraction is an important tool for multivariate data analysis. A number of methods have been proposed in the literature. In what follows, we will review a large family of feature extraction methods for learning linear transformations and then explain their characteristics.

2.1. Problem Setup. We start by a general setup for feature extraction learning on data of multiple views and their class labels, and then explain their representations in a common space.

Let $\{(\mathbf{x}_i^{(1)}, \dots, \mathbf{x}_i^{(v)}, \mathbf{y}_i)\}_{i=1}^n$ be a dataset of v views, where the i th data points $\mathbf{x}_i^{(s)} \in \mathbb{R}^{d_s}$ of all views ($1 \leq s \leq v$) are assumed to share the same class labels in \mathbf{y}_i of c labels.

The labels can have different interpretations, dependent of the underlying learning task. For multi-output regression, $\mathbf{y}_i \in \mathbb{R}^c$, and it reduces to a scalar for the classical regression for which $c = 1$. For multi-label classification, $\mathbf{y}_i \in \{0, 1\}^c$ with an understanding that the i th data points of all views have the class label r if $(\mathbf{y}_i)_r = 1$ and otherwise 0, where $(\mathbf{y}_i)_r$ is the r th entry of \mathbf{y}_i . If $\mathbf{1}_c^T \mathbf{y}_i = 1$, then multi-label classification becomes a problem of c -class classification since one and only one class label is assigned to each instance of data points of all views. In particular, if $c = 2$ and $\mathbf{1}_c^T \mathbf{y}_i = 1$, then it is just the binary classification.

For the purpose of feature extraction learning, objective fulfilling linear transformations are sought to extract the latent representation for each view. Let $P_s \in \mathbb{R}^{d_s \times k}$ be the projection matrix for view s to transform $\mathbf{x}_i^{(s)}$ from \mathbb{R}^{d_s} to $\mathbf{z}_i^{(s)} = P_s^T \mathbf{x}_i^{(s)}$ in the common space \mathbb{R}^k . Represent the n data points of view s by $X_s = [\mathbf{x}_1^{(s)}, \dots, \mathbf{x}_n^{(s)}] \in \mathbb{R}^{d_s \times n}$ and its latent representation by $Z_s = [\mathbf{z}_1^{(s)}, \dots, \mathbf{z}_n^{(s)}] = P_s^T X_s \in \mathbb{R}^{k \times n}$. Accordingly, we denote the centered matrix and the sample mean of view s , and the label matrix by

$$(2) \quad \widehat{X}_s = X_s H_s, \quad \mathbf{m}_s = \frac{1}{n} X_s \mathbf{1}_n, \quad Y = [\mathbf{y}_1, \dots, \mathbf{y}_n],$$

respectively, where $H_n = I_n - \frac{1}{n} \mathbf{1}_n \mathbf{1}_n^T$.

The sample cross-covariance between view s and view t is given by

$$(3) \quad C_{s,t} = \frac{1}{n} X_s H_n X_t^T.$$

In particular, $C_{s,s}$ is the covariance of view s . It is not so hard to verify that

$$\begin{aligned} \widehat{X}_s &= X_s - \mathbf{m}_s \mathbf{1}^T = [\mathbf{x}_1^{(s)} - \mathbf{m}_s, \dots, \mathbf{x}_n^{(s)} - \mathbf{m}_s], \\ C_{s,t} &= \frac{1}{n} \widehat{X}_s \widehat{X}_t^T = \frac{1}{n} \sum_{i=1}^n (\mathbf{x}_i^{(s)} - \mathbf{m}_s)(\mathbf{x}_i^{(t)} - \mathbf{m}_t)^T, \end{aligned}$$

upon noticing $H_n^2 = H_n$.

For the c -class classification, i.e., $Y \in \{0,1\}^{c \times n}$ and $\mathbf{1}_c^T \mathbf{y}_i = 1$, we have the following properties:

$$(4) \quad Y^T \mathbf{1}_c = \mathbf{1}_n, \Sigma = YY^T = \text{diag}(n_1, \dots, n_c),$$

where $n_r = \sum_{i=1}^n (\mathbf{y}_i)_r$ is the number of data points in class r . Denote by \mathbf{u}_r^T the r th row of Y , and define

$$(5) \quad \mathbf{m}_s^r := \frac{1}{n_r} X_s \mathbf{u}_r, \forall r,$$

the mean of all data points in view s having class label r . So, we have $\sum_{r=1}^c \mathbf{u}_r = Y^T \mathbf{1}_c = \mathbf{1}_n$. The between-class scatter matrix S_b^s can be written as

$$(6) \quad S_b^s = X_s \left(Q - \frac{1}{n} \mathbf{1}_n \mathbf{1}_n^T \right) X_s^T,$$

where

$$Q = Y^T \Sigma^{-1} Y = \sum_{r=1}^c \frac{1}{n_r} \mathbf{u}_r \mathbf{u}_r^T.$$

To see (6), we note, by definition, that

$$\begin{aligned} S_b^s &= \sum_{r=1}^c n_r \mathbf{m}_s^r (\mathbf{m}_s^r)^T - n \mathbf{m}_s \mathbf{m}_s^T \\ &= \sum_{r=1}^c n_r (\mathbf{m}_s^r - \mathbf{m}_s) (\mathbf{m}_s^r - \mathbf{m}_s)^T, \end{aligned}$$

where we have used

$$\sum_{r=1}^c n_r \mathbf{m}_s^r = \sum_{r=1}^c X_s \mathbf{u}_r = X_s \mathbf{1}_n = n \mathbf{m}_s$$

and $\sum_{r=1}^c n_r = n$. Since $S_w^s = nC_{s,s} - S_b^s$, the within-class scatter matrix takes the form

$$(7) \quad S_w^s = X_s (I - Q) X_s^T.$$

A graph Laplacian is a matrix representation of a graph and popularly used to approximate the manifold structure of data via locality information encoded by the edge weights of the undirected graph. Denote $G_s = (V_s, E_s, W_s)$ built for X_s , where $V_s = \{1, \dots, n\}$ is the graph nodes and $W_s = [w_{i,j}^{(s)}] \in \mathbb{R}^{n \times n}$ is symmetric with its entry $w_{i,j}^{(s)}$ being the weight of edge $(i, j) \in E_s$. The graph Laplacian matrix of G_s is defined as $L_s = D_s - W_s$, where $D_s = \text{diag}(W_s \mathbf{1}_n)$. The manifold approximation is captured by

$$(8) \quad \frac{1}{2} \sum_{i=1}^n \sum_{j=1}^n w_{i,j}^{(s)} \|\mathbf{z}_i^{(s)} - \mathbf{z}_j^{(s)}\|^2 = \text{tr}(P_s^T X_s L_s X_s^T P_s).$$

By minimizing (8) with respect to P_s , the optimal projection matrix P_s satisfies the following criterion: if $\mathbf{x}_i^{(s)}$ is close to $\mathbf{x}_j^{(s)}$, i.e., the similarity $w_{i,j}^{(s)}$ is large, the distance between two corresponding projected points, $\mathbf{z}_i^{(s)}$ and $\mathbf{z}_j^{(s)}$, is also small in the projected space.

We point out that S_b^s and S_w^s in (6) and (7) can be expressed in terms of some graph Laplacians as

$$(6') \quad S_b^s = -X_s L_s X_s^T, \quad W_s = Q - \frac{1}{n} \mathbf{1}_n \mathbf{1}_n^T,$$

$$(7') \quad S_w^s = X_s L_s X_s^T, \quad W_s = Q.$$

In fact, S_w^s of (7') was used in the Fisher score for supervised feature selection [27], and both S_b^s and S_w^s here were used in [28] with modified weight matrices to incorporate local information.

2.2. Single-view Feature Extraction. A series of single-view (i.e., $v = 1$) feature extraction methods that learn a linear transformation matrix have been proposed. Principal component analysis (PCA) seeks the directions of the input space so that the variance of the projected data is maximized. The joint optimization to obtain transformation matrix P_1 is formulated as

$$(9) \quad \max_{P_1 \in \mathbb{R}^{d_1 \times k}} \text{tr}(P_1^T C_{1,1} P_1) : \text{s. t. } P_1^T P_1 = I_k.$$

PCA is an unsupervised method since it does not incorporate any output data, and so PCA projections may not be consistent with output data.

For multi-class classification, linear discriminant analysis (LDA) incorporates output labels to search a projection matrix so that the within-class scatter is minimized while the between-class scatter is maximized. The commonly used LDA formulation is

$$(10) \quad \max_{P_1 \in \mathbb{R}^{d_1 \times k}} \text{tr}(P_1^T S_b^1 P_1) : \text{s. t. } P_1^T N P_1 = I_k.$$

It is popular, in large part because it admits an analytic solution as a generalized eigenvalue problem, where N is either S_w^1 or $C_{1,1}$. Another approach is the trace ratio formulation for the same purpose

$$(11) \quad \max_{P_1 \in \mathbb{R}^{d_1 \times k}} \frac{\text{tr}(P_1^T S_b^1 P_1)}{\text{tr}(P_1^T M P_1)} : \text{s. t. } P_1^T N P_1 = I_k,$$

where M and N can be one of $C_{1,1}$, S_w^1 and I_n . Some of the interesting combinations are as follows:

- (1) (11) with $M = C_{1,1}$ [15] or with $M = S_w^1$ [16] to obtain an orthonormal projection matrix by letting $N = I_{d_1}$,
- (2) (11) with $M = S_w^1$ and $N = C_{1,1}$ to learn uncorrelated directions [29, 30],
- (3) (11) with $M = C_{1,1}$ and $N = S_w^1$, equivalent to (10) since $nC_{1,1} = S_w^1 + S_b^1$,
- (4) (11) with $M = N \neq I_{d_1}$, reducing to (10).

Another special case is with $M = N = I_{d_1}$ to give

$$(12) \quad \max_{P_1 \in \mathbb{R}^{d_1 \times k}} \text{tr}(P_1^T S_b^1 P_1) : \text{s. t. } P_1^T P_1 = I_k.$$

For multi-output regression and multi-label classification, partial least squares (PLS) and canonical correlation analysis (CCA) are two common approaches that also learn projection matrices for output data. PLS looks for a projection matrix that maximizes the cross-covariance between the projected input and output:

$$(13a) \quad \max_{P_1 \in \mathbb{R}^{d_1 \times k}, P_Y \in \mathbb{R}^{c \times k}} \text{tr}(P_1^T X_1 H_n Y^T P_Y)$$

$$(13b) \quad \text{s. t. } P_1^T P_1 = P_Y^T P_Y = I_k,$$

where $P_Y \in \mathbb{R}^{c \times k}$ is the projection matrix for the output. CCA also maximizes the cross-correlation

$$(14a) \quad \max_{P_1 \in \mathbb{R}^{d_1 \times k}, P_Y \in \mathbb{R}^{c \times k}} \text{tr}(P_1^T X_1 H_n Y^T P_Y)$$

$$(14b) \quad \text{s. t. } P_1^T C_{1,1} P_1 = P_Y^T Y Y^T P_Y = I_k,$$

except that they have different constraints. Manifold learning can be used for feature extraction in both supervised and unsupervised settings depending on how the graph is constructed. In [31], a general framework called graph embedding [31] is formulated as

$$(15a) \quad \min_{P_1} \text{tr}(P_1^T X_1 L_1 X_1^T P_1)$$

$$(15b) \quad \text{s. t. } P_1^T X_1 B X_1^T P_1 = I_k \text{ or } P_1^T P_1 = I_k,$$

where B is to be specified. According to (6') and (7'), PCA (9) and LDA (10) are special cases of (15), but the trace ratio formulation (11) is not. Locality preserving projection (LPP) [32] is (15) with graph Laplacian matrix $L_1 = D_1 - W_1$, and $B = \text{diag}(W_1 \mathbf{1}_n)$, while Laplacian eigenmap (LE) [33] solves LPP directly for $P_1^T X_1$ instead of P_1 . As stated in [31], locally linear embedding (LLE) [34] and ISOMAP [35] are also special cases of (15).

2.3. Multi-view Feature Extraction. As multiple inputs may come from different sources (views), they are most likely heterogeneous and have large discrepancy. The aim of multi-view feature extraction is to exploit consensual, complementary, and overlapping information among different views.

PLS (13) and CCA (14) can be directly applied to two-view data ($v = 2$) simply by replacing Y and P_Y in (13) or (14) with X_2 and P_2 of view 2, respectively. For $v > 2$, the multi-set CCA (MCCA) [5]

$$(16a) \quad \max_{\{P_s \in \mathbb{R}^{d_s \times k}\}} \sum_{s=1}^v \sum_{t=1}^v \text{tr}(P_s^T C_{s,t} P_t)$$

$$(16b) \quad \text{s. t. } \sum_{s=1}^v P_s^T C_{s,s} P_s = I_k,$$

is the most popularly used, chiefly due to its analytic solution via the generalized eigen-decomposition that has been well studied [36, 37]. Orthogonal multiset CCA (OMCCA)

$$(17a) \quad \max_{\{P_s \in \mathbb{R}^{d_s \times k}\}} \sum_{s=1}^v \sum_{t=1}^v \frac{\text{tr}(P_s^T C_{s,t} P_t)}{\sqrt{\text{tr}(P_s^T C_{s,s} P_s)} \sqrt{\text{tr}(P_t^T C_{t,t} P_t)}}$$

$$(17b) \quad \text{s. t. } P_s^T P_s = I_k, \forall s$$

is proposed in [23]. Its special case $v = 2$ is the orthogonal CCA (OCCA) [12, 21, 22]. In [24], a variant of (17) was studied. The key in (16) and (17) is the use of pairwise cross-covariance matrices $\{C_{s,t}\}$ to capture the consensus among the v views.

Recently, PLS is extended for $v > 2$ in [25], too, where the orthogonality constraints $P_s^T P_s = I_k$ for all s are imposed.

For supervised learning, the output label Y can be naturally considered as one input view [11]. However, the special structure of label information is neglected. To

compensate that negligence and to take full advantage of label data, sophisticated multi-view feature extraction methods have been proposed. In [8], generalized multi-view analysis (GMA) is formulated, by integrating LDA (or some variants of it) and CCA, as

$$(18a) \quad \max_{\{P_s\}} \sum_{s=1}^v \text{tr}(P_s^T S_b^s P_s) + \sum_{s=1}^v \sum_{t=1, t \neq s}^v \alpha_{s,t} \text{tr}(P_s^T C_{s,t} P_t)$$

$$(18b) \quad \text{s. t. } P_s^T S_w^s P_s = I_k, \forall s,$$

where $\alpha_{s,t}$ is the weight for cross-covariance between view s and view t . Unfortunately, this is a difficult optimization problem whose KKT condition leads to a multi-parameter eigenvalue problem like (36) later for which there is no efficient numerical method for its solution. For that reason, authors in [8] proposed to solve, instead, a relaxed problem: the same objective but a constraint different from (18b):

$$(19) \quad \sum_{s=1}^v \gamma_s P_s^T S_w^s P_s = I_k,$$

resulting in a generalized eigenvalue problem [37], where γ_s are parameters to balance v independent constraints. S_b^s and S_w^s can be the ones in (6') and (7') for the classical LDA, or those in [28, 31]. Multi-view uncorrelated linear discriminant analysis (MULDA) [10] was proposed to replace (18b) with the uncorrelated constraints

$$(20) \quad \sum_{s=1}^v \gamma_s P_s^T C_{s,s} P_s = I_k.$$

Multi-view modular discriminant analysis (MvMDA) [9] aims to maximize the distances between different class centers across different views and minimize the within-class scatter

$$(21a) \quad \max_{\{P_s\}} \sum_{s=1}^v \sum_{t=1}^v \text{tr}(P_s^T X_s A X_t^T P_t)$$

$$(21b) \quad \text{s. t. } \sum_{s=1}^v P_s^T S_w^s P_s = I_k,$$

where $A = Y^T \Sigma^{-1} H_c \Sigma^{-1} Y$.

It is worth noting that imposing orthogonality constraints has attracted much attention in multi-view feature extraction in unsupervised learning, but it is seldom explored in supervised learning. In addition, it has been widely studied in single-view methods in both unsupervised and supervised learning.

3. ORTHOGONAL MULTI-VIEW ANALYSIS

In this section, we propose a novel unified framework for multi-view discriminant analysis in order to learn orthogonal projections onto a latent common space.

3.1. Motivation. An orthogonal projection is able to preserve the pairwise distance if the vectors to be projected live in the range of the projection. Specifically, if $\mathbf{x}_i^{(s)} \in \mathcal{R}(P_s)$ for all i and $P_s^T P_s = I_k$, then we have $\mathbf{x}_i^{(s)} = P_s \tilde{\mathbf{z}}_i^{(s)}$ for some $\tilde{\mathbf{z}}_i^{(s)}$ and

$$P_s \mathbf{z}_i^{(s)} = P_s (P_s^T \mathbf{x}_i^{(s)}) = P_s \underbrace{P_s^T P_s}_{I_k} \tilde{\mathbf{z}}_i^{(s)} = P_s \tilde{\mathbf{z}}_i^{(s)} = \mathbf{x}_i^{(s)}.$$

Now, the pairwise Euclidean distance between $\mathbf{x}_i^{(s)}$ and $\mathbf{x}_j^{(s)}$

$$(22) \quad \|\mathbf{x}_i^{(s)} - \mathbf{x}_j^{(s)}\|^2 = \|P_s(\mathbf{z}_i^{(s)} - \mathbf{z}_j^{(s)})\|^2 = \|\mathbf{z}_i^{(s)} - \mathbf{z}_j^{(s)}\|^2$$

is preserved in the projected space. Distance preservation as an important learning criterion has been successfully used in single-view dimensionality reduction with kernel representation [19] and Bayesian estimation [20].

Orthogonal projection has been explored in LDA (11) with $N = I_{d_1}$ in [15, 16] for single-view feature extraction, and in CCA with two views [12, 21, 22] and MCCA with more than two views [23, 24] for multi-view feature extraction. However, imposing orthogonality constraints has not yet been well studied for supervised multi-view subspace learning.

3.2. A Unified Framework. We propose a novel unified orthogonal multi-view subspace learning (OMvSL) framework in the trace ratio formulation given by

$$(23a) \quad \max_{\{P_s\}} \sum_{s=1}^v \sum_{t=1}^v \frac{\text{tr}(P_s^T \Phi_{s,t} P_t)}{\sqrt{\text{tr}(P_s^T \Psi_{s,s} P_s)} \sqrt{\text{tr}(P_t^T \Psi_{t,t} P_t)}}$$

$$(23b) \quad \text{s. t. } P_s^T P_s = I_k, \forall s,$$

where $\Psi_{s,s}$ for $s = 1, \dots, v$ are positive semi-definite matrices. As stated in [15], the trace ratio formulation is an essential formulation for general dimensionality reduction and may lead to solutions that are superior to the ones from the ratio trace formulation.

The proposed OMvSL (23) encompasses OLDA and OMCCA as special cases:

- (1) For $v = 1$, (23) with $\Psi_{1,1} = S_b^1$ and $\Phi_{1,1} = M$ reduces to OLDA (11).
- (2) For $v \geq 2$, (23) with $\Phi_{s,t} = C_{s,t}$ and $\Psi_{s,s} = C_{s,s}$ becomes OMCCA (17).

OMvSL (23) can be used to inspire various models in the form of trace ratio formulations. We shall present various novel models instantiated from OMvSL (23) for multi-view discriminant analysis in subsection 3.3 and multi-label classification in subsection 3.4.

OMvSL is a versatile framework, but it presents a difficult optimization problem to solve. Generic optimization techniques [38, 39, 40] can always be applied, but they ignore the special form in the objective, are usually not so efficient as customized algorithms, and, worst of all, are not practically feasible even for datasets of modest scale. In Section 5, we will present a successive approximation algorithm that approximately solves OMvSL efficiently.

It is tempting to modify OMvSL (23) by adding

$$(24) \quad P_s^T \Psi_{s,s} P_s = I_k, \forall s,$$

to eliminate the denominators in the objective in hope for a simpler problem to solve. But (24) and (23b) may conflict. To see that, we note that $P_s^T \Psi_{s,s} P_s \succeq \lambda_{\min} P_s^T P_s$ where λ_{\min} is the smallest eigenvalue of $\Psi_{s,s}$, and so if $\lambda_{\min} > 1$, then there is no way to satisfy both (24) and (23b) at the same time. On the other hand,

(23a) with (24) but not (23b) bears similarity to existing models of the ratio trace formulation in subsection 2.3.

3.3. Novel Multi-view Discriminant Analysis Models. Three orthogonal multi-view discriminant analysis models are proposed, inspired by existing models similar to (23) for multi-class classification where $\mathbf{y}_i \in \{0, 1\}^c$ and $\mathbf{y}_i^T \mathbf{1}_c = 1$ [8, 9, 10]. Each new model is intrinsically different from its corresponding existing model due to the trace ratio formulation (23a) and orthogonality constraints (23b).

Orthogonal GMA. The proposed orthogonal variant of GMA (18), called *Orthogonal GMA* (OGMA), is (23) with

$$(25a) \quad \Phi_{s,t} = \begin{cases} S_b^s, & s = t, \\ \alpha_{s,t} C_{s,t}, & s \neq t, \end{cases}$$

$$(25b) \quad \Psi_{s,s} = S_w^s.$$

Orthogonal MLDA. The proposed orthogonal variant of MLDA (18a) with (20), called *Orthogonal MLDA* (OMLDA), is (23) with (25a) and

$$(26) \quad \Psi_{s,s} = C_{s,s}.$$

Orthogonal MvMDA. The proposed orthogonal variant of MvMDA (21), called *Orthogonal MvMDA* (OMvMDA), is (23) with

$$(27) \quad \Phi_{s,t} = A, \quad \Psi_{s,s} = S_w^s.$$

3.4. Novel Multi-view Multi-label Classification Models. In multi-view multi-label classification, the output $\mathbf{y}_i \in \{0, 1\}^c$ with c labels and $\{\mathbf{x}_i^{(1)}, \dots, \mathbf{x}_i^{(v)}, \mathbf{y}_i\}_{i=1}^n$ is the paired data. Under the proposed framework (23), we can come up the following two strategies to incorporate output data for multi-view multi-label classification:

Orthogonal Multi-view Multi-label CCA (OM²CCA). This approach is proposed to take the output labels in $Y = [\mathbf{y}_1, \dots, \mathbf{y}_n] \in \{0, 1\}^{c \times n}$ as the $(v+1)$ st view $X_{v+1} := Y$ in OMCCA [11]. Together with v input views, there are $v+1$ views. OMCCA is employed to learn projection matrices $\{P_s\}$ and $P_{v+1} := P_Y$ in a latent common space. This idea has been explored for $v = 1$ in [11, 12, 23]. OMCCA is instantiated from (23) with

$$(28a) \quad \Phi_{s,t} = \begin{cases} 0, & s = t, \\ C_{s,t}, & s \neq t, \end{cases}$$

$$(28b) \quad \Psi_{s,s} = C_{s,s},$$

for $s, t = 1, \dots, v+1$, where $C_{s,v+1} = X_s H Y = C_{v+1,s}^T$.

Orthogonal Hilbert-Schmidt Independence Criterion (OHSIC). This approach is proposed to take the HSIC criterion [41] for learning embedding of each input view. The estimator of HSIC is defined as

$$(29) \quad \text{HSIC}(Z_s, Y) = \frac{1}{(n-1)^2} \text{tr}(Z_s^T Z_s H_n Y^T Y H_n),$$

where $Z_s = P_s^T X_s$ and $Z_s^T Z_s$ is the linear kernel of the projected data of view s . To achieve the best alignment between Z_s and Y , the maximization of HSIC with respect to P_s is expected. The proposed HSIC method is instantiated from (23)

with

$$(30a) \quad \Phi_{s,t} = \begin{cases} X_s H_n Y^T Y H_n X_s^T, & s = t, \\ \alpha_{s,t} C_{s,t}, & s \neq t, \end{cases}$$

$$(30b) \quad \Psi_{s,s} = C_{s,s},$$

for $s, t = 1, \dots, v$. Different from (28), this approach does not learn P_Y .

4. AN EIGENVALUE ALGORITHM

Currently there is no numerically efficient method to solve OMvSL (23), especially for high-dimensional datasets. In preparing for presenting a successive approximation method in the next section, in what follows we will outline a Krylov subspace method that is suitable for computing the top eigenpair for the generalized eigenvalue problem. To simplify notation, we will explain the method generically for

$$(31) \quad A\mathbf{x} = \lambda B\mathbf{x} \quad \text{with} \quad \mathbf{x} \in \mathcal{R}(B),$$

where $A, B \in \mathbb{R}^{d \times d}$ are symmetric, $\mathcal{R}(A) \subseteq \mathcal{R}(B)$, $B \succeq 0$. Suppose that matrix-vector products, $A\mathbf{x}$ and $B\mathbf{x}$ for any given \mathbf{x} , are the only operations that can be done numerically.

The Krylov subspace method will serve as the workhorse of our successive approximation algorithm that approximately solves OMvSL (23). It is worth noting that B may be singular and will be singular in our applications. A common past practice in data science is simply to perturb B to $B + \epsilon I_d$ for some tiny $\epsilon > 0$ as a regularization and solve $A\mathbf{x} = \lambda(B + \epsilon I_d)\mathbf{x}$ instead. While this successfully gets rid of the singularity issue, it may create a more serious one in that the eventually computed top eigenvector likely falls into the null spaces of A and B and is thus useless for the underlying application.

The method is the so-called Locally Optimal Block Preconditioned Extended Conjugate Gradient method (LOBPECG) [42, Algorithm 2.3] which combines LOBPCG of Knyazev [43] and the *inverse free Krylov subspace method* of Golub and Ye [44]. For our current application, we will simply use the version without preconditioning and blocking. Algorithm 1 outlines an adaption of [42, Algorithm 2.3] for (31).

A few comments regarding this algorithm and its efficient implementation are in order:

- (1) There is no need to use $\|A\|_2$ and $\|B\|_2$ exactly. Some very rough estimates are just good enough so long as the estimates have the same magnitudes, respectively.
- (2) At line 2, it is to make sure $\mathbf{x}_1 \in \mathcal{R}(B)$.
- (3) There are two parameters to choose: the order n_{kry} of the Krylov space (32) and the stopping tolerance tol . There is no easy way to determine what the optimal n_{kry} is. In general, the larger n_{kry} is, the faster the convergence, but then more work in generating the orthonormal basis matrix Z . Usually $n_{\text{kry}} = 10$ is good. For applications that required accuracy is not too stringent, $\text{tol} = 10^{-6}$ is often more than adequate.
- (4) The orthonormal basis matrix Z can be efficiently computed by the symmetric Lanczos process [45]. For better numerical stability in making sure $Z^T Z = I$ within the working precision, re-orthogonalization may be necessary.

Algorithm 1 Locally Optimal Extended Conjugate Gradient method (LOECG)

Input: eigenvalue problem (31), n_{kry} , tolerance tol ;

Output: top eigenpair (λ, \mathbf{x}) .

- 1: pick a random $\mathbf{x}_1 \in \mathbb{R}^d$;
 - 2: $\mathbf{x}_1 = B\mathbf{x}_1$, $\mathbf{x}_1 = \mathbf{x}_1/\|\mathbf{x}_1\|_2$, $\rho = \mathbf{x}_1^T A\mathbf{x}_1/\mathbf{x}_1^T B\mathbf{x}_1$;
 - 3: $\mathbf{r} = A\mathbf{x}_1 - \rho B\mathbf{x}_1$, $\text{res} = \|\mathbf{r}\|_2/(\|A\|_2 + |\rho|\|B\|_2)$;
 - 4: $\mathbf{x}_0 = 0$;
 - 5: **while** $\text{res} \geq \text{tol}$ **do**
 - 6: compute an orthonormal basis matrix Z of the Krylov subspace
 - (32) $\mathcal{R}(Z) = \mathcal{R}([\mathbf{x}_1, (A - \rho B)\mathbf{x}_1, \dots, (A - \rho B)^{n_{\text{kry}}}\mathbf{x}_1])$;
 - 7: $\mathbf{p} = \mathbf{x}_0 - Z(Z^T \mathbf{x}_0)$, $W = [Z, \mathbf{p}/\|\mathbf{p}\|_2]$;
 - 8: compute the top eigenpair (ρ, \mathbf{z}) of $W^T A W - \lambda W^T B W$, where $\|\mathbf{z}\|_2 = 1$;
 - 9: $\mathbf{x}_0 = \mathbf{x}_1$;
 - 10: $\mathbf{x}_1 = W\mathbf{z}$, $\mathbf{r} = A\mathbf{x}_1 - \rho B\mathbf{x}_1$, $\text{res} = \|\mathbf{r}\|_2/(\|A\|_2 + |\rho|\|B\|_2)$;
 - 11: **end while**
 - 12: **return** (ρ, \mathbf{x}_1) .
-

- (5) At line 7, some guard step must be taken. For example, in the first iteration $\mathbf{x}_0 = 0$ and so $\mathbf{p} = 0$. We should just let $W = Z$. In the subsequent iterations, we will have to test whether \mathbf{x}_0 is in or nearly in $\mathcal{R}(Z)$. For that purpose, we need another tolerance, e.g., if $\|\mathbf{p}\|_2 \leq 10^{-12}$, then we will regard already $\mathbf{x}_0 \in \mathcal{R}(Z)$ and set $W = Z$; otherwise, re-orthogonalize \mathbf{p} against Z : $\mathbf{p} = \mathbf{p} - Z(Z^T \mathbf{p})$ to make sure $W^T W = I$ within the working precision.
- (6) At line 8, AW and BW , except their last columns, are likely already computed at the time of generating Z at line 6. They should be reused here to save work.
- (7) The eigenvalue problem for $W^T A W - \lambda W^T B W$ is of very small size $(n_{\text{kry}} + 1) \times (n_{\text{kry}} + 1)$ at most and also $W^T B W \succ 0$ as guaranteed by Lemma 4.1 below. It can be solved by first computing the Cholesky decomposition $W^T B W = R^T R$ and then the full eigen-decomposition of $R^{-T}(W^T A W)R^{-1}$. Finally, $\mathbf{z} = R^{-1}\mathbf{w}$, where \mathbf{w} is the top eigenvector of $R^{-T}(W^T A W)R^{-1}$.

Lemma 4.1. *In Algorithm 1, $\mathcal{R}(W) \subseteq \mathcal{R}(B)$ and thus $W^T B W \succ 0$.*

Proof. Initially, after line 2, $\mathbf{x}_1 \in \mathcal{R}(B)$. Therefore at (32), $\mathcal{R}(Z) \subseteq \mathcal{R}(B)$ because $\mathcal{R}(A) \subseteq \mathcal{R}(B)$. In the first iteration of the **while**-loop, $\mathbf{x}_0 = 0$ and $W = Z$ and so $\mathcal{R}(W) \subseteq \mathcal{R}(B)$, $\mathbf{x}_0, \mathbf{x}_1 \in \mathcal{R}(B)$. Inductively, each time at the beginning of executing the **while**-loop, we have $\mathbf{x}_0, \mathbf{x}_1 \in \mathcal{R}(B)$. So we will have at line 7, $\mathbf{p} \in \mathcal{R}(B)$ and $\mathcal{R}(Z) \subseteq \mathcal{R}(B)$, implying $\mathcal{R}(W) \subseteq \mathcal{R}(B)$. Consequently, at the conclusion of executing the **while**-loop, we still have $\mathbf{x}_0, \mathbf{x}_1 \in \mathcal{R}(B)$.

Since $B \succeq 0$ and $\mathcal{R}(W) \subseteq \mathcal{R}(B)$, $W^T B W$ must be positive definite. \square

5. ALGORITHM FOR OMvSL

For ease of presentation, we rewrite OMvSL (23) as

$$(33) \quad \max_{\{P_s\}} g(\{P_s\}) : \text{s. t. } P_s^T P_s = I_k, \mathcal{R}(P_s) \subseteq \mathcal{R}(\Psi_{s,s}) \forall s,$$

where

$$g(\{P_s\}) := \sum_{s=1}^v \sum_{t=1}^v \frac{\text{tr}(P_s^T \Phi_{s,t} P_t)}{\sqrt{\text{tr}(P_s^T \Psi_{s,s} P_s)} \sqrt{\text{tr}(P_t^T \Psi_{t,t} P_t)}}.$$

For $k = 1$, all P_s are column vectors. By convention that we use lowercase letters for vectors, we will replace them by \mathbf{p}_s instead. Since $g(\{\mathbf{p}_s\})$ is homogeneous in each \mathbf{p}_s , i.e., $g(\{\mathbf{p}_s/\alpha_s\}) \equiv g(\{\mathbf{p}_s\})$ for any scalar $\alpha_s > 0$, the constraints $\mathbf{p}_s^T \mathbf{p}_s = 1$ is inconsequential. In fact, (33) is equivalent to

$$(34) \quad \max_{\{\mathbf{p}_s \in \mathbb{R}^{n_s}\}} f(\{\mathbf{p}_s\}) : \text{s.t. } \mathbf{p}_s^T \Psi_{s,s} \mathbf{p}_s = 1, \mathbf{p}_s \in \mathcal{R}(\Psi_{s,s}) \forall s,$$

where $f(\{\mathbf{p}_s\})$ is given by

$$(35) \quad f(\{\mathbf{p}_s\}) := \sum_{s=1}^v \sum_{t=1}^v \mathbf{p}_s^T \Phi_{s,t} \mathbf{p}_t.$$

The KKT condition of (34) gives rise to a multi-parameter eigenvalue problem:

$$(36a) \quad \mathcal{A} \mathbf{p} = \mathcal{B} \Lambda \mathbf{p}, \mathbf{p} \in \mathcal{R}(\mathcal{B}),$$

where

$$(36b) \quad \mathcal{A} = \begin{bmatrix} \Phi_{11} & \Phi_{12} & \cdots & \Phi_{1v} \\ \Phi_{21} & \Phi_{22} & \cdots & \Phi_{2v} \\ \vdots & \vdots & \ddots & \vdots \\ \Phi_{v1} & \Phi_{v2} & \cdots & \Phi_{vv} \end{bmatrix}, \mathcal{B} = \begin{bmatrix} \Psi_{11} & & & \\ & \Psi_{22} & & \\ & & \ddots & \\ & & & \Psi_{vv} \end{bmatrix},$$

$$(36c) \quad \Lambda = \begin{bmatrix} \lambda_1 I_{n_1} & & & \\ & \lambda_2 I_{n_2} & & \\ & & \ddots & \\ & & & \lambda_v I_{n_v} \end{bmatrix}, \mathbf{p} = \begin{bmatrix} \mathbf{p}_1 \\ \vdots \\ \mathbf{p}_v \end{bmatrix}.$$

This is also a long standing problem in statistics, and there is no existing numerical technique that is readily available to solve it with guarantee. Existing methods include variations of the power method for matrix eigenvalues [46], which are simple to use but often slowly convergent, and adaptations of common optimization techniques onto Riemannian manifolds to solve (34) [47, 48], which often converge faster but use the gradient or even Hessian of f and, as a result, are not particularly well suited for large scale problems. None of those methods guarantee to deliver the global optimum of (34).

In many real-world applications, an approximate solution is just as good as a very accurate solution. A relaxed problem to (34) is

$$(37) \quad \max_{\{\mathbf{q}_s\}} f(\{\mathbf{q}_s\}) : \text{s.t. } \sum_{s=1}^v \mathbf{q}_s^T \Psi_{s,s} \mathbf{q}_s = 1, \mathbf{q}_s \in \mathcal{R}(\Psi_{s,s}).$$

The KKT condition for (37) is

$$(38) \quad \mathcal{A} \mathbf{q} = \lambda \mathcal{B} \mathbf{q}, \mathbf{q} \in \mathcal{R}(\mathcal{B})$$

which is a generalized eigenvalue problem that has been well studied, where \mathcal{A} and \mathcal{B} are as given by (36b). Often

$$\mathcal{R}(\mathcal{A}) \subseteq \mathcal{R}(\mathcal{B})$$

which we will assume in this paper and the top eigenvector \mathbf{q} is the maximizer of (37). Even though \mathcal{B} is positive semi-definite, it is possible that \mathcal{B} is singular. In the previous section, we discussed a common practice and its fatal shortcoming for the underlying data science application. Algorithm 1 in section 4 can be applied to solve (38) for its top eigenpair in such a way that singular \mathcal{B} does not matter, without regularization.

We propose to construct an approximation solution for (34), and thereby for (33) with $k = 1$, from the solution to (37) for $k = 1$ as follows. Let $(\lambda_1, \mathbf{q}^{\text{opt}} = [\mathbf{q}_s^{\text{opt}}])$ with $\mathbf{q}_s^{\text{opt}} \in \mathbb{R}^{d_s}$ be the top eigenpair of the eigenvalue problem (38). An approximate solution is then constructed by

$$(39) \quad \gamma_s = \|\mathbf{q}_s^{\text{opt}}\|_2, \mathbf{p}_s^{\text{opt}} = \mathbf{q}_s^{\text{opt}}/\gamma_s, \forall s.$$

This solves (33) with $k = 1$ approximately, or finds an approximation to the first columns of optimal P_s of (33). Suppose that approximations to the first ℓ columns, say $\mathbf{p}_s^{(j)} \in \mathbb{R}^{d_s}$ for $1 \leq j \leq \ell$, of nearly optimal P_s of (33) are obtained and $\ell < k$. Let

$$(40) \quad P_s^{(\ell)} = [\mathbf{p}_s^{(1)}, \mathbf{p}_s^{(2)}, \dots, \mathbf{p}_s^{(\ell)}] \in \mathbb{R}^{d_s \times \ell}, \forall s.$$

It is reasonable to assume

$$(41) \quad [P_s^{(\ell)}]^\top P_s^{(\ell)} = I_\ell, \mathcal{R}(P_s^{(\ell)}) \subseteq \mathcal{R}(\Psi_{s,s}), \forall s.$$

We propose to find the next columns of nearly optimal P_s for all s of (33) by solving

$$(42a) \quad \max_{\{\mathbf{q}_s \in \mathbb{R}^{n_s}\}} f(\{\mathbf{q}_s\}) : \text{s.t.} \quad \sum_{s=1}^v \mathbf{q}_s^\top \Psi_{s,s} \mathbf{q}_s = 1, \mathbf{q}_s \in \mathcal{R}(\Psi_{s,s}) \forall s,$$

$$(42b) \quad \mathbf{q}_s^\top P_s^{(\ell)} = 0 \forall s,$$

and then normalize each \mathbf{q}_s of the optimizer of (42) as in (39) to construct the next $\mathbf{p}_s^{(\ell+1)}$.

Theorem 1. *Given $P_s^{(\ell)}$ as in (40) satisfying (41), problem (42) is equivalent to*

$$(43) \quad \max_{\{\mathbf{q}_s \in \mathbb{R}^{n_s}\}} f_\ell(\{\mathbf{q}_s\}) : \text{s.t.} \quad \sum_{s=1}^v \mathbf{q}_s^\top \Psi_{s,s}^{(\ell)} \mathbf{q}_s = 1, \mathbf{q}_s \in \mathcal{R}(\Psi_{s,s}^{(\ell)}) \forall s,$$

where

$$(44a) \quad \Pi_s^{(\ell)} = I_{n_s} - P_s^{(\ell)} [P_s^{(\ell)}]^\top,$$

$$(44b) \quad \Phi_{s,t}^{(\ell)} = \Pi_s^{(\ell)} \Phi_{s,t} \Pi_t^{(\ell)}, \Psi_{s,s}^{(\ell)} = \Pi_s^{(\ell)} \Psi_{s,s} \Pi_s^{(\ell)},$$

$$(44c) \quad f_\ell(\{\mathbf{q}_s\}) = \sum_{s,t} \mathbf{q}_s^\top \Phi_{s,t}^{(\ell)} \mathbf{q}_t.$$

Proof. We will show that the feasible sets for (42) and (43) are the same and $f(\{\mathbf{q}_s\}) = f_\ell(\{\mathbf{q}_s\})$ for any vector $\{\mathbf{q}_s\}$ in the feasible set.

Let $\{\mathbf{q}_s\}$ satisfy the constraints of (42). Since $\mathbf{q}_s^\top P_s^{(\ell)} = 0$, we have $\Pi_s^{(\ell)} \mathbf{q}_s = \mathbf{q}_s$. Since $\mathbf{q}_s \in \mathcal{R}(\Psi_{s,s}) = \mathcal{R}(\Psi_{s,s}^{1/2})$ where $\Psi_{s,s}^{1/2}$ is the unique positive semi-definite square

root of $\Psi_{s,s}$, we have $\mathbf{q}_s = \Psi_{s,s}^{1/2} \mathbf{w}_s$ for some \mathbf{w}_s . Therefore

$$\begin{aligned} \mathbf{q}_s &= \Pi_s^{(\ell)} \mathbf{q}_s = \Pi_s^{(\ell)} \Psi_{s,s}^{1/2} \mathbf{w}_s \\ &\in \mathcal{R}(\Pi_s^{(\ell)} \Psi_{s,s}^{1/2}) = \mathcal{R}(\Pi_s^{(\ell)} \Psi_{s,s} \Pi_s^{(\ell)}), \\ \mathbf{q}_s^\top \Phi_{s,t} \mathbf{q}_t &= [\Pi_s^{(\ell)} \mathbf{q}_s]^\top \Phi_{s,t} [\Pi_s^{(\ell)} \mathbf{q}_t] = \mathbf{q}_s^\top \Phi_{s,t}^{(\ell)} \mathbf{q}_t. \end{aligned}$$

Hence $\{\mathbf{q}_s\}$ satisfies the constraints of (43) and $f(\{\mathbf{q}_s\}) = f_\ell(\{\mathbf{q}_s\})$. On the other hand, let $\{\mathbf{q}_s\}$ satisfy the constraints of (43). Since $\mathbf{q}_s \in \mathcal{R}(\Psi_{s,s}^{(\ell)}) = \mathcal{R}(\Pi_s^{(\ell)} \Psi_{s,s}^{1/2})$, we have $\mathbf{q}_s = \Pi_s^{(\ell)} \Psi_{s,s}^{1/2} \mathbf{w}_s$ for some \mathbf{w}_s and therefore

$$\begin{aligned} \mathbf{q}_s^\top P_s^{(\ell)} &= \mathbf{w}_s^\top \Psi_{s,s}^{1/2} \Pi_s^{(\ell)} P_s^{(\ell)} = 0, \\ \mathbf{q}_s &= \Psi_{s,s}^{1/2} \mathbf{w}_s - P_s^{(\ell)} [P_s^{(\ell)}]^\top \Psi_{s,s}^{1/2} \mathbf{w}_s \in \mathcal{R}(\Psi_{s,s}^{1/2}) = \mathcal{R}(\Psi_{s,s}). \end{aligned}$$

That $\mathbf{q}_s^\top P_s^{(\ell)} = 0$ implies $\Pi_s^{(\ell)} \mathbf{q}_s = \mathbf{q}_s$ for all s , and therefore

$$\mathbf{q}_s^\top \Phi_{s,t} \mathbf{q}_t = \mathbf{q}_s^\top \Pi_s^{(\ell)} \Phi_{s,t} \Pi_t^{(\ell)} \mathbf{q}_t = \mathbf{q}_s^\top \Phi_{s,t}^{(\ell)} \mathbf{q}_t.$$

Hence also $\{\mathbf{q}_s\}$ satisfies the constraints of (42) and $f(\{\mathbf{q}_s\}) = f_\ell(\{\mathbf{q}_s\})$. \square

In view of our previous discussion, problem (43) is equivalent to finding the top eigenpair of

$$(45) \quad \mathcal{A}^{(\ell)} \mathbf{q} = \lambda \mathcal{B}^{(\ell)} \mathbf{q} \quad \text{with } \mathbf{q} \in \mathcal{R}(\mathcal{B}^{(\ell)}),$$

where $\mathcal{A}^{(\ell)}$ and $\mathcal{B}^{(\ell)}$ take the same form as \mathcal{A} and \mathcal{B} in (36b), except with all $\Phi_{s,t}$ and $\Psi_{s,s}$ replaced by $\Phi_{s,t}^{(\ell)}$ and $\Psi_{s,s}^{(\ell)}$, respectively. Note now that $\mathcal{B}^{(\ell)}$ is guaranteed singular for $\ell > 1$ because for each s ,

$$\begin{aligned} \text{rank}(\Psi_{s,s}^{(\ell)}) &= \text{rank}(\Pi_s^{(\ell)} \Psi_{s,s}^{1/2}) \\ &\leq \min\{\text{rank}(\Pi_s^{(\ell)}), \text{rank}(\Psi_{s,s}^{1/2})\} \\ &\leq \text{rank}(\Pi_s^{(\ell)}) = n_s - \ell. \end{aligned}$$

Hence the range constraint $\mathbf{q} \in \mathcal{R}(\mathcal{B}^{(\ell)})$ is indispensable. Any straightforward application of existing eigen-computation routine to $\mathcal{A}^{(\ell)} - \lambda \mathcal{B}^{(\ell)}$ will likely encounter some numerical issue. Note that $\mathbf{q} \in \mathcal{R}(\mathcal{B}^{(\ell)})$ is equivalent to $\mathbf{q}_s \in \mathcal{R}(\Psi_{s,s}^{(\ell)}) \forall s$ in (43).

Algorithm 2 summarizes our range constrained successive approximation method for solving OMvSL, which calls Algorithm 1 to compute the top eigenvector of $\mathcal{A}^{(\ell)} - \lambda \mathcal{B}^{(\ell)}$, where $\mathcal{A}^{(\ell)} \equiv \mathcal{A}$ and $\mathcal{B}^{(\ell)} \equiv \mathcal{B}$ for $\ell = 0$.

According to Algorithm 1, the efficiency of Algorithm 2 critically depends on the execution of matrix-vector products by $\mathcal{A}^{(\ell)}$ and $\mathcal{B}^{(\ell)}$. Noting that how $\mathcal{A}^{(\ell)}$ and $\mathcal{B}^{(\ell)}$ are defined, together with (44a) and (44b), we find that

$$\mathcal{A}^{(\ell)} = \Pi^{(\ell)} \mathcal{A} \Pi^{(\ell)}, \quad \mathcal{B}^{(\ell)} = \Pi^{(\ell)} \mathcal{B} \Pi^{(\ell)},$$

where $\Pi^{(\ell)} = \text{diag}(\Pi_1^\ell, \dots, \Pi_s^\ell)$. Thus $\mathbf{y} := \mathcal{X}^{(\ell)} \mathbf{x}$ where \mathcal{X} is either \mathcal{A} or \mathcal{B} can be done in three steps:

$$(46a) \quad \mathbf{x} \leftarrow \Pi^{(\ell)} \mathbf{x},$$

$$(46b) \quad \mathbf{y} \leftarrow \mathcal{X} \mathbf{x},$$

$$(46c) \quad \mathbf{y} \leftarrow \Pi^{(\ell)} \mathbf{y}.$$

Algorithm 2 OSAVE: Orthogonal Successive Approximation via Eigenvectors

Input: $\{\Phi_{s,t} \in \mathbb{R}^{d_s \times n_t}, 1 \leq s, t \leq v\}$, $\{\Psi_{s,s} \in \mathbb{R}^{d_s \times d_s}, 1 \leq s \leq v\}$, integer $1 \leq k \leq \min\{d_1, \dots, d_v\}$;
Output: $\{P_s \in \mathbb{O}^{d_s \times k}\}$, the set of most correlated matrices.
1: compute the top eigenvector $[\mathbf{q}_1^T, \mathbf{q}_2^T, \dots, \mathbf{q}_v^T]^T$ of $\mathcal{A} - \lambda\mathcal{B}$ by Algorithm 1, where $\mathbf{q}_s \in \mathbb{R}^{d_s}$;
2: $\mathbf{p}_s^{(1)} = \mathbf{q}_s / \|\mathbf{q}_s\|_2$ for $s = 1, 2, \dots, v$;
3: **for** $\ell = 1, 2, \dots, k-1$ **do**
4: compute the top eigenvector $[\mathbf{q}_1^T, \mathbf{q}_2^T, \dots, \mathbf{q}_v^T]^T$ of $\mathcal{A}^{(\ell)} - \lambda\mathcal{B}^{(\ell)}$ by Algorithm 1, where $\mathbf{q}_s \in \mathbb{R}^{d_s}$;
5: $\mathbf{p}_s^{(\ell+1)} = \mathbf{q}_s / \|\mathbf{q}_s\|_2$ for $s = 1, 2, \dots, v$;
6: **end for**
7: $P_s = [\mathbf{p}_s^{(1)}, \dots, \mathbf{p}_s^{(k)}]$ for $s = 1, 2, \dots, v$;
8: **return** $\{P_s \in \mathbb{O}^{d_s \times k}\}$.

The operations in (46a) and (46c) are the same one, and should be implemented as follows. In the case of (46a), write $\mathbf{x} = [\mathbf{x}_1^T, \dots, \mathbf{x}_v^T]^T$ where $\mathbf{x}_s \in \mathbb{R}^{n_s}$ and do

$$\mathbf{x}_s \leftarrow \mathbf{x}_s - P_s^{(\ell)} ([P_s^{(\ell)}]^T \mathbf{x}_s) \quad \forall s,$$

where the bracket must be respected for maximum computational efficiency. The operation in (46b) can be broken into many mini-ones $\Phi_{s,t}\mathbf{x}_t$, $\Psi_{s,s}\mathbf{x}_s$ for all s, t whose calculations depend on the structures in $\Phi_{s,t}$ and $\Psi_{s,s}$ from the underlying task. While it is impossible for us to offer recommendations on a very general setting, a frequent scenario where OMvSL is needed has $\Phi_{s,t}$ and $\Psi_{s,s}$ taking the form

$$(47a) \quad \Phi_{s,t} = A_s A_t^T, \quad \Psi_{s,s} = B_s B_s^T$$

where

$$(47b) \quad A_s = A_s^{\text{raw}} \left(I_{m_a} - \frac{1}{m_a} \mathbf{1}_{m_a} \mathbf{1}_{m_a}^T \right) \in \mathbb{R}^{d_s \times m_a},$$

$$(47c) \quad B_s = B_s^{\text{raw}} \left(I_{m_s} - \frac{1}{m_s} \mathbf{1}_{m_s} \mathbf{1}_{m_s}^T \right) \in \mathbb{R}^{d_s \times m_s}.$$

Here A_s^{raw} and B_s^{raw} represent raw input data matrices from an application, which may also be sparse. In such a scenario, A_s and B_s should not be formed explicitly in a large scale application, i.e., at least one of d_s , m_a , and m_s is large, say in the tens of thousands or more, and neither should $\Phi_{s,t}$ and $\Psi_{s,s}$. As an example, $\mathbf{y}_s := \Phi_{s,t}\mathbf{x}_t$ can be executed in the order as follows:

$$\mathbf{z} \leftarrow (A_t^{\text{raw}})^T \mathbf{x}_t, \mathbf{z} \leftarrow \mathbf{z} - \frac{\mathbf{1}_{m_a}^T \mathbf{z}}{m_a} \mathbf{1}_{m_a}, \mathbf{y}_s \leftarrow A_s^{\text{raw}} \mathbf{z}.$$

To get a sense of the computational complexity of OSAVE (Algorithm 2), in what follows we present a rough estimate, assuming $\Phi_{s,t}$ and $\Psi_{s,s}$ are given and dense. For the ℓ th loop: lines 3–6 of Algorithm 2 which calls Algorithm 1, we have, for the leading cost terms for one loop of Algorithm 1 (lines 6–10),

- (a) matrix-vector products by $\mathcal{A}^{(\ell)}$ and $\mathcal{B}^{(\ell)}$: $2n_{\text{nkrv}}(d^2 + \sum_s d_s^2 + 8dl)$,
- (b) orthogonalization in generating W : $6dn_{\text{nkrv}}$ if by the Lanczos process or $2dn_{\text{nkrv}}^2$ if also with full reorthogonalization (recommended),

(c) forming $W^T AW$ and $W^T BW$ (assuming AW and BW built along the way are reused): $4dn_{\text{kry}}^2$,

(d) solving $W^T AW - \lambda W^T BW$: $14n_{\text{kry}}^3$ [37, p.500].

Here $d = \sum_s d_s$ and these estimates work for $\ell = 0$, i.e., line 1 of Algorithm 2, too. For simplicity, let us assume that on average Algorithm 1 takes m iterations to finish, and full reorthogonalization is used for robustness. Then the overall complexity estimate is

$$(48) \quad m \left\{ kn_{\text{kry}} \left[2d^2 + \sum_s d_s^2 + 6dn_{\text{kry}} \right] + 8n_{\text{kry}} dk^2 \right\} \approx 2mkn_{\text{kry}} d^2,$$

where we have dropped the cost in solving $W^T AW - \lambda W^T BW$ due to that n_{kry} is usually of $O(1)$, and we have assumed $k \ll d$ in practice. Further improvement in complexity is possible if A_s and B_s in (47) are very sparse, and then d^2 in (48) can be replaced by the total number of nonzero entries in A_s and B_s for all s .

6. EXPERIMENTS

In this section, we will evaluate the effectiveness of our proposed models instantiated from the unified framework (23) by comparing with existing methods on two learning tasks: multi-view feature extraction and multi-view multi-label classification.

TABLE 1. Datasets for feature extraction (followed by classification), where the number of features for each view is shown inside the bracket.

Dataset	samples	class	view 1	view 2	view 3	view 4	view 5	view 6
mfeat	2000	10	fac (216)	fon (76)	kar (64)	mor (6)	pix (240)	zer (47)
Caltech101-7	1474	7	CENTRIST (254)	GIST (512)	LBP (1180)	HOG (1008)	CH (64)	SIFT-SPM (1000)
Caltech101-20	2386	20	CENTRIST (254)	GIST (512)	LBP (1180)	HOG (1008)	CH (64)	SIFT-SPM (1000)
Scene15	4310	15	CENTRIST (254)	GIST (512)	LBP (531)	HOG (360)	SIFT-SPM (1000)	-
Reuters	18758	6	English(21531)	France (24892)	German (34251)	Italian (15506)	Spanish (11547)	-
Ads	3279	2	url+alt+caption (588)	origurl (495)	ancurl (472)	-	-	-

6.1. Multi-view Feature Extraction.

6.1.1. *Datasets.* Six datasets in Table 1 are used to evaluate the performance of the proposed models: OGMA, OMLDA, and OMvMDA in terms of multi-view feature extraction. We apply various feature descriptors, including CENTRIST [49], GIST [50], LBP [51], histogram of oriented gradient (HOG), color histogram (CH), and SIFT-SPM [52], to extract features of views for image datasets: Caltech101¹[53] and Scene15² [52]. Note that we drop CH for Scene15 due to the gray-level images. Multiple Features (mfeat)³, Internet Advertisements (Ads)⁴, and Reuters⁵ are publicly available from UCI machine learning repository. The dataset mfeat contains handwritten numeral data with six views including profile correlations (fac), Fourier coefficients of the character shapes (fou), Karhunen-Love coefficients (kar), morphological features (mor), pixel averages in 2×3 windows (pix), and Zernike moments (zer). Ads is used to predict whether or not a given hyperlink (associated with an image) is an advertisement and has three views: features based on the terms in the images URL, caption, and alt text (url+alt+caption), features based on the terms in the URL of the current site (origurl), and features based on the terms in the anchor URL (ancurl). Reuters is a multi-view text categorization dataset containing feature characteristics of documents originally written in five languages (English, French, German, Italian, and Spanish) and their translations over a common set of six categories (C15, CCAT, E21, ECAT, GCAT, and M11). Only a subset of Reuters, those written in English and their translations in other four languages, is used. As the feature dimension of Reuters is too big to handle by the baseline methods, a preprocessing step is performed by PCA to keep 500 features per view.

6.1.2. *Compared methods.* As shown in Subsection 3.3, our proposed models, although instantiated from the proposed framework (23), are inspired by some of the existing ones. Hence, the three proposed models have close counterparts via solving generalized eigenvalue problems. Specifically, the compared methods include

- GMA [8]
- MLDA and MLDA-m with modifications [10]
- MvMDA [9]
- MULDA and MULDA-m with modifications [10]
- OGMA: the proposed model instantiated from (23) with (25)
- OMLDA: the proposed model instantiated from (23) with (25a) and (26)
- OMvMDA: the proposed model instantiated from (23) with (27).

Except for MvMDA and OMvMDA, all methods share the same trade-off parameter to balance the pairwise correlation and supervised information. In our experiments, we set $\alpha_{s,t} = \alpha, \forall s \neq t$ so as to reduce the complexity of model selection and tune $\alpha \in \{0.01, 0.1, 1, 10, 100\}$ for proper balance in supervised setting. To prevent the singularity of matrices $\{\Psi_{s,s}\}$, we add a diagonal matrix with a small value, e.g., 10^{-8} , to $\Psi_{s,s} \forall s$ for all compared methods.

¹http://www.vision.caltech.edu/Image_Datasets/Caltech101/

²https://figshare.com/articles/15-Scene_Image_Dataset/7007177

³<https://archive.ics.uci.edu/ml/datasets/Multiple+Features>

⁴<https://archive.ics.uci.edu/ml/datasets/internet+advertisements>

⁵<https://archive.ics.uci.edu/ml/datasets/Reuters+RCV1+RCV2+Multilingual,+Multiview+Text+Categorization+Test+collection>

TABLE 2. Means and standard deviations of accuracy by the 1-nearest neighbor classifier on embeddings by 9 methods on 6 multi-view datasets over 10 random draws from each dataset (10% training and 90% testing).

method	mfeat	Ads	Scene15	Caltech101-7	Caltech101-20	Reuters
GMA	0.9399 ± 0.0087	0.9261 ± 0.0176	0.6166 ± 0.0120	0.9325 ± 0.0104	0.8130 ± 0.0106	0.8369 ± 0.0047
MLDA	0.9284 ± 0.0052	0.9309 ± 0.0079	0.5468 ± 0.0137	0.9229 ± 0.0079	0.7659 ± 0.0117	0.7911 ± 0.0050
MvMDA	0.9378 ± 0.0091	0.7796 ± 0.0360	0.6088 ± 0.0146	0.9265 ± 0.0078	0.8050 ± 0.0132	0.8367 ± 0.0041
MULDA	0.9523 ± 0.0046	0.9249 ± 0.0352	0.5789 ± 0.0121	0.9265 ± 0.0083	0.8220 ± 0.0109	0.7529 ± 0.0081
MLDA-m	0.9309 ± 0.0079	0.9418 ± 0.0061	0.5699 ± 0.0120	0.8978 ± 0.0098	0.7377 ± 0.0114	0.7939 ± 0.0051
MULDA-m	0.9512 ± 0.0044	0.9282 ± 0.0362	0.5795 ± 0.0154	0.9259 ± 0.0099	0.8217 ± 0.0058	0.7589 ± 0.0081
OGMA (proposed)	0.9609 ± 0.0060	0.9412 ± 0.0114	0.7359 ± 0.0156	0.9501 ± 0.0052	0.8600 ± 0.0103	0.8360 ± 0.0039
OMLDA (proposed)	0.9571 ± 0.0064	0.9410 ± 0.0115	0.7547 ± 0.0105	0.9498 ± 0.0048	0.8685 ± 0.0100	0.8353 ± 0.0037
OMvMDA (proposed)	0.9599 ± 0.0063	0.9423 ± 0.0103	0.7198 ± 0.0191	0.9471 ± 0.0072	0.8428 ± 0.0102	0.8347 ± 0.0037

6.1.3. *Classification.* To evaluate the learning performance of compared methods, the 1-nearest neighbor classifier as the base classifier is employed. We run each method to learn projection matrices by varying the dimension of the common subspace $k \in [2, 30]$ for all datasets except for mfeat with $k \in [2, 6]$ due to the smallest view of 6 features. We split the data into training and testing with ratio 10/90. The learned projection matrices are used to transform both training and testing data into the latent common space, and then classifier is trained and tested in this space. Following [24, 23, 12], the serial feature fusion strategy is employed by concatenating projected features from all views. Classification accuracy is used to measure the learning performance. Experimental results are reported in terms of the average and standard deviation over 10 randomly drawn splits.

Table 2 shows the best results of 9 compared methods on 6 multi-view datasets with 10% training and 90% testing over all tested k s and α s (the analysis on parameter sensitivity and training sample size will be discussed in subsections 6.1.4 and 6.1.5, respectively). From Table 2, we have the following observations: (i) our proposed models instantiated from (23) generally outperform their counterparts that solve some relaxed generalized eigenvalue problems. Although GMA produces the best results on Reuters, the differences compared to each of the three proposed methods are all marginal; (ii) three proposed models demonstrate best results on different datasets, while OGMA and OMLDA perform consistently better than OMvMDA on five of six datasets. This empirically shows that the model hypothesis in each model is data-dependent.

6.1.4. *Parameter Sensitivity Analysis.* The sensitivity analyses on parameters k and α are performed by varying one of them while recording the best average accuracy over the other within its testing range.

Figure 1 shows the results of 9 methods on six datasets as k varies. Most compared methods demonstrate the increasing trend when k increases. The proposed methods produce consistently better accuracies than others. On Ads, Caltech101-7 and Reuters, our methods show the saturation on accuracy, while MvMDA shows a significant drop after the certain k on four of six datasets.

We further investigate the impact of parameter α on GMA, OGMA, MLDA and OMLDA except MvMDA and OMvMDA since both methods does not contain parameter α . In Figure 2, GMA and OGMA demonstrates quite robust to α , and the best accuracy can be obtained around $\alpha = 10^{-2}$. However, MLDA and OMLDA are quite sensitive to α and the accuracy decreases significantly especially for $\alpha > 0.1$. These observations imply that more contribution from pairwise correlation may hurt MLDA and OMLDA, but no noticeable impact on GMA and OGMA. Over all tested α s, our proposed methods outperform their counterparts.

6.1.5. *Impact on Training Sample Size.* We further show the impact of training sample size on the compared methods by varying the ratio of training data from 10% to 60%. The best average results over 10 randomly drawn splits are reported. Fig. 3 shows the accuracy improves when the training ratio is increasing on Ads and Caltech101-7. It is observed that (i) all methods show better performance when training sample size increases, (ii) our proposed methods show consistently better results than others, and (iii) all methods converge to similar results when training sample size becomes very large except MvMDA.

6.2. Multi-view Multi-label Classification.

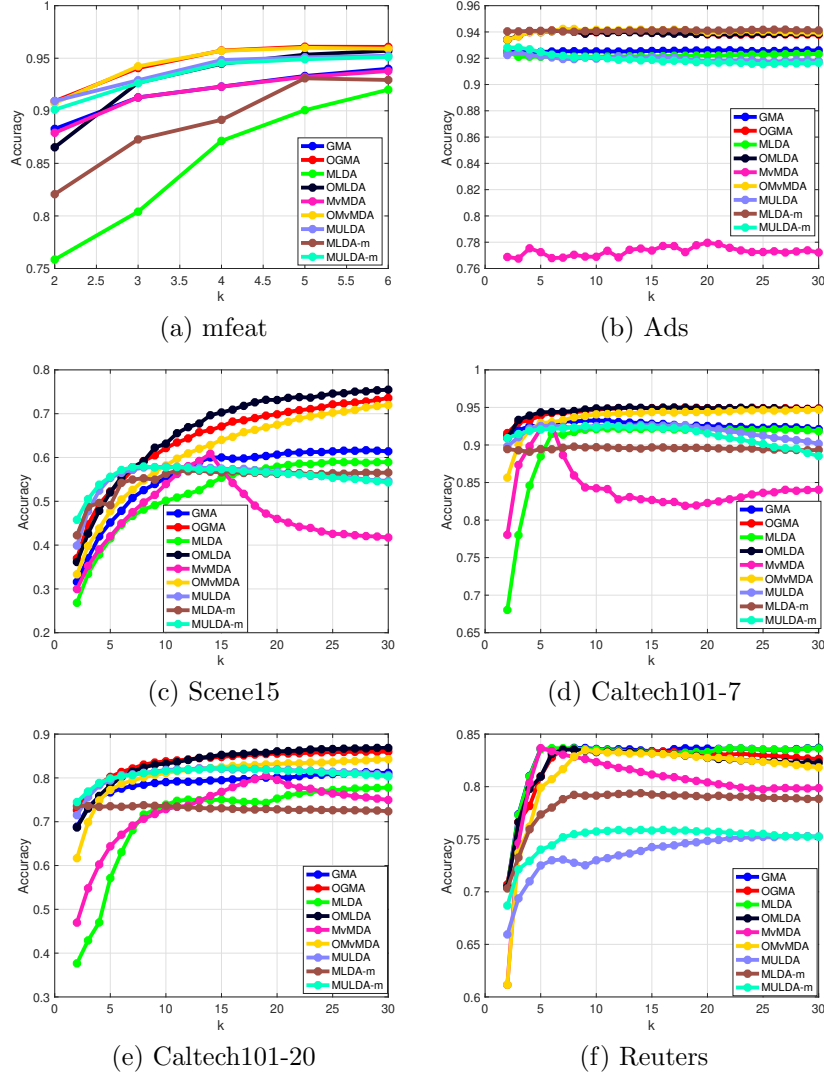


FIGURE 1. Classification accuracy of 9 methods on 6 datasets over 10 random splits (10% training and 90% testing), as k varies.

TABLE 3. Multi-view multi-label datasets for classification

	samples	labels	views
emotions	593	6	2
Corel5k	4999	260	7
espgame	20770	268	7
iaprtc12	19627	291	7
mirflickr	25000	38	7
pascal07	9963	20	7

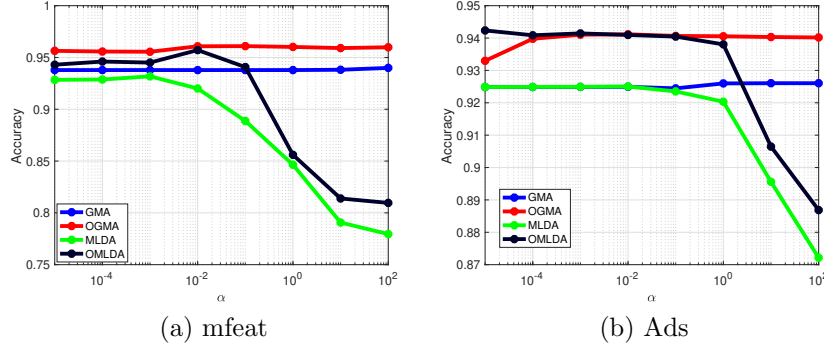


FIGURE 2. Classification accuracy by 4 methods on mfeat and Ads over 10 random splits (10% training and 90% testing), as α varies in $[10^{-5}, 10^2]$.

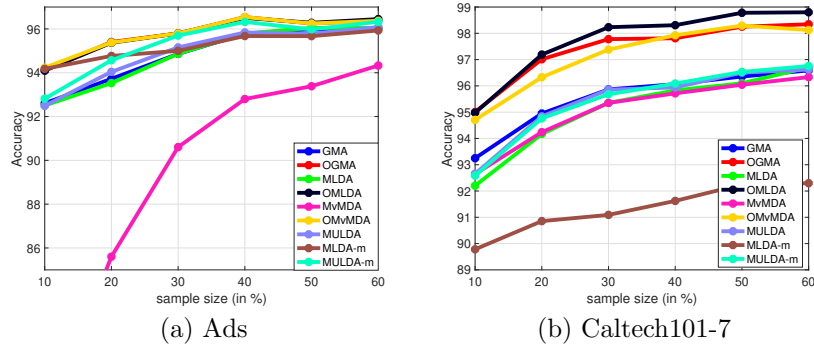


FIGURE 3. Classification accuracy by all 9 methods on Ads and Scene15 as the ratio of training data varies from 10% to 60%.

6.2.1. *Datasets.* The statistics of six publicly available datasets are shown in Table 3, which are employed to evaluate the proposed methods for multi-view multi-label classification. Dataset emotions⁶ has two feature views: 8 rhythmic attributes and 64 timbre attributes. Core15k [54] is a benchmark dataset for keyword based image retrieval and image annotation. Dataset espgame [55] is obtained from an online game where two players gain points by agreeing on words describing the image. Dataset iaprtc12 [55] is a set of images accompanied with descriptions in several languages for cross-lingual retrieval. Both pascal07 [56] and mirflickr [57] are collected from the Flickr website. The last five datasets have been preprocessed with various feature descriptors and are publicly available⁷ [58, 59]. In our experiments, we choose 7 descriptors: DenseHue (100), DenseHueV3H1 (300), DenseSift (1000), Gist (512), HarrisHue (100), HarrisHueV3H1 (300), and HarrisSift (1000).

6.2.2. *Compared Methods.* Multi-label classification [60] is a variant of the classification problem, where one instance may have various numbers of labels from a

⁶<http://mulan.sourceforge.net>

⁷<http://lear.inrialpes.fr/people/guillaumin/data.php>

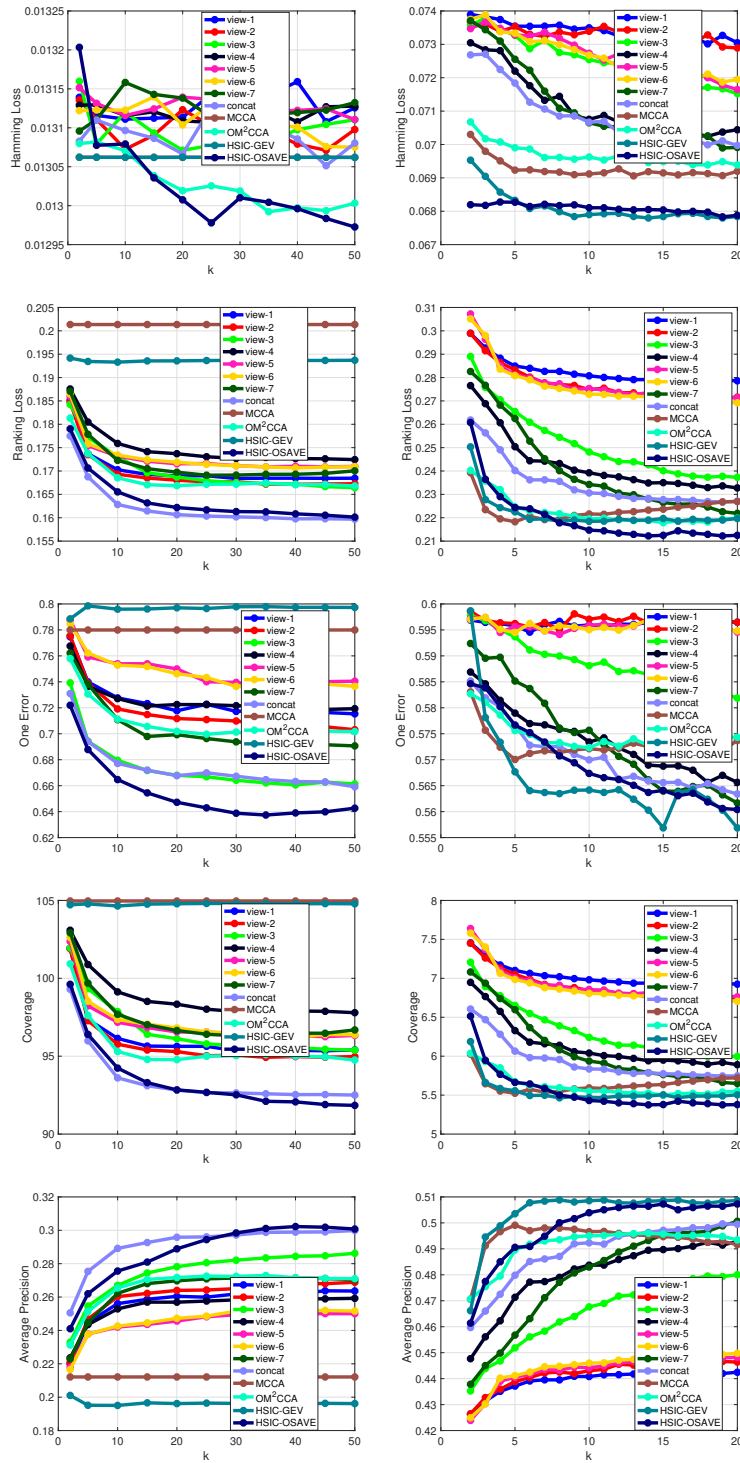


FIGURE 4. Results with respect to five metrics by compared methods on Core15k (top row) and pascal07 (bottom row) over 10 random splits (10% training and 90% testing), as k varies.

TABLE 4. Results in terms of the 5 metrics on the six datasets (10% for training and 90% for testing over 10 random splits). Best results are in bold.

	method	Hamming Loss ↓	Ranking Loss ↓	One Error ↓	Coverage ↓	Average Precision ↑
emotions	view-1	0.3060 ± 0.0156	0.3038 ± 0.0195	0.4672 ± 0.0312	2.4903 ± 0.1790	0.6647 ± 0.1319
	view-2	0.3403 ± 0.0247	0.4392 ± 0.0173	0.5949 ± 0.0422	3.1069 ± 0.0625	0.5678 ± 0.0625
	concat	0.3046 ± 0.0155	0.3596 ± 0.0279	0.4869 ± 0.0359	2.8039 ± 0.1208	0.6290 ± 0.1091
	MCCA	0.3661 ± 0.0267	0.4554 ± 0.0188	0.6399 ± 0.0321	3.1830 ± 0.1291	0.5468 ± 0.1291
	OM ² CCA	0.3006 ± 0.0124	0.3249 ± 0.0346	0.4948 ± 0.0488	2.5740 ± 0.1779	0.6492 ± 0.1777
	HSIC-GEV	0.3646 ± 0.0241	0.4547 ± 0.0105	0.6223 ± 0.0466	3.0798 ± 0.1888	0.5553 ± 0.1888
	OHSIC	0.2953 ± 0.0110	0.3079 ± 0.0248	0.4655 ± 0.0342	2.4850 ± 0.1222	0.6662 ± 0.1222
Corel5k	view-1	0.0131 ± 0.0001	0.1684 ± 0.0031	0.7153 ± 0.0147	95.3444 ± 1.4930	0.2637 ± 1.5828
	view-2	0.0131 ± 0.0001	0.1672 ± 0.0034	0.7031 ± 0.0110	94.9287 ± 1.6843	0.2689 ± 1.6548
	view-3	0.0131 ± 0.0001	0.1664 ± 0.0033	0.6606 ± 0.0072	95.3894 ± 1.7478	0.2862 ± 1.7478
	view-4	0.0131 ± 0.0000	0.1724 ± 0.0030	0.7187 ± 0.0154	97.7932 ± 1.6951	0.2592 ± 1.6252
	view-5	0.0131 ± 0.0000	0.1709 ± 0.0027	0.7366 ± 0.0107	96.2485 ± 1.4062	0.2502 ± 1.4062
	view-6	0.0131 ± 0.0000	0.1707 ± 0.0025	0.7365 ± 0.0137	96.2007 ± 1.3439	0.2520 ± 1.3704
	view-7	0.0131 ± 0.0000	0.1691 ± 0.0026	0.6906 ± 0.0065	96.3108 ± 1.3974	0.2716 ± 1.5536
	concat	0.0131 ± 0.0001	0.1597 ± 0.0040	0.6591 ± 0.0135	92.5057 ± 2.1126	0.2999 ± 2.1126
	MCCA	0.0131 ± 0.0000	0.2013 ± 0.0020	0.7799 ± 0.0115	104.9648 ± 1.4837	0.2121 ± 1.4837
	OM ² CCA	0.0130 ± 0.0000	0.1668 ± 0.0028	0.6982 ± 0.0106	94.7535 ± 1.4380	0.2729 ± 1.4651
	HSIC-GEV	0.0131 ± 0.0000	0.1933 ± 0.0031	0.7885 ± 0.0161	104.6444 ± 1.5763	0.2011 ± 1.6329
OHSIC	0.0130 ± 0.0001	0.1601 ± 0.0026	0.6374 ± 0.0126	91.8414 ± 1.5051	0.3022 ± 1.3774	
iaprtc12	view-1	0.0196 ± 0.0000	0.1871 ± 0.0012	0.6746 ± 0.0047	142.9013 ± 0.9209	0.2216 ± 0.8681
	view-2	0.0196 ± 0.0000	0.1850 ± 0.0014	0.6611 ± 0.0041	141.9732 ± 1.0396	0.2272 ± 1.1048
	view-3	0.0195 ± 0.0000	0.1738 ± 0.0012	0.6262 ± 0.0066	137.2026 ± 0.6685	0.2535 ± 0.6685
	view-4	0.0196 ± 0.0000	0.1768 ± 0.0009	0.6375 ± 0.0024	138.5784 ± 0.6618	0.2508 ± 0.6618
	view-5	0.0197 ± 0.0000	0.1879 ± 0.0010	0.6902 ± 0.0039	143.2122 ± 0.7937	0.2179 ± 0.7937
	view-6	0.0197 ± 0.0000	0.1862 ± 0.0013	0.6802 ± 0.0033	142.4131 ± 0.9414	0.2233 ± 0.9414
	view-7	0.0196 ± 0.0000	0.1720 ± 0.0013	0.6341 ± 0.0049	136.0222 ± 0.7975	0.2587 ± 0.7975
	concat	0.0195 ± 0.0000	0.1696 ± 0.0010	0.6218 ± 0.0032	134.6660 ± 0.7990	0.2649 ± 0.8544
	MCCA	0.0196 ± 0.0000	0.1804 ± 0.0109	0.6447 ± 0.0252	140.0515 ± 5.4482	0.2400 ± 5.0702
	OM ² CCA	0.0196 ± 0.0000	0.1709 ± 0.0011	0.6220 ± 0.0030	135.2006 ± 0.8948	0.2559 ± 0.9850
	HSIC-GEV	0.0195 ± 0.0001	0.1648 ± 0.0022	0.5893 ± 0.0035	132.1792 ± 1.2844	0.2776 ± 1.2844
OHSIC	0.0195 ± 0.0000	0.1673 ± 0.0009	0.6078 ± 0.0025	133.6776 ± 0.7331	0.2661 ± 0.7209	
espgame	view-1	0.0174 ± 0.0000	0.2150 ± 0.0011	0.6762 ± 0.0052	134.8974 ± 0.5372	0.2235 ± 0.5178
	view-2	0.0174 ± 0.0000	0.2144 ± 0.0013	0.6766 ± 0.0058	134.6899 ± 0.6207	0.2238 ± 0.6207
	view-3	0.0175 ± 0.0000	0.2035 ± 0.0009	0.7213 ± 0.0049	129.8373 ± 0.4775	0.2185 ± 0.6298
	view-4	0.0175 ± 0.0000	0.2030 ± 0.0012	0.7129 ± 0.0032	129.1738 ± 0.7794	0.2201 ± 0.7794
	view-5	0.0174 ± 0.0000	0.2157 ± 0.0009	0.6668 ± 0.0051	135.3101 ± 0.4779	0.2262 ± 0.4854
	view-6	0.0174 ± 0.0000	0.2159 ± 0.0009	0.6687 ± 0.0033	135.4435 ± 0.4592	0.2252 ± 0.5143
	view-7	0.0175 ± 0.0000	0.2054 ± 0.0006	0.7279 ± 0.0049	130.7208 ± 0.5104	0.2160 ± 0.5104
	concat	0.0175 ± 0.0000	0.2015 ± 0.0010	0.6989 ± 0.0063	128.8904 ± 0.6606	0.2283 ± 0.6859
	MCCA	0.0174 ± 0.0001	0.2136 ± 0.0061	0.6784 ± 0.0518	134.1460 ± 1.9614	0.2249 ± 1.9531
	OM ² CCA	0.0174 ± 0.0000	0.2076 ± 0.0008	0.6283 ± 0.0040	132.0874 ± 0.5329	0.2454 ± 0.5074
	HSIC-GEV	0.0174 ± 0.0000	0.2068 ± 0.0010	0.6236 ± 0.0053	131.9247 ± 0.6241	0.2481 ± 0.6241
OHSIC	0.0174 ± 0.0000	0.2061 ± 0.0010	0.6207 ± 0.0053	131.5208 ± 0.5965	0.2495 ± 0.5965	
mirflickr	view-1	0.1224 ± 0.0004	0.1798 ± 0.0014	0.4960 ± 0.0041	15.3929 ± 0.0753	0.4993 ± 0.0734
	view-2	0.1220 ± 0.0002	0.1780 ± 0.0014	0.4872 ± 0.0033	15.3257 ± 0.0511	0.5054 ± 0.0613
	view-3	0.1177 ± 0.0004	0.1614 ± 0.0012	0.4259 ± 0.0031	14.5379 ± 0.0488	0.5451 ± 0.0488
	view-4	0.1186 ± 0.0003	0.1672 ± 0.0013	0.4414 ± 0.0046	14.8891 ± 0.0513	0.5329 ± 0.0513
	view-5	0.1227 ± 0.0004	0.1815 ± 0.0013	0.5053 ± 0.0040	15.4924 ± 0.0535	0.4933 ± 0.0641
	view-6	0.1226 ± 0.0003	0.1805 ± 0.0011	0.5027 ± 0.0045	15.4430 ± 0.0631	0.4963 ± 0.0631
	view-7	0.1171 ± 0.0006	0.1592 ± 0.0016	0.4263 ± 0.0036	14.3775 ± 0.0864	0.5471 ± 0.0864
	concat	0.1170 ± 0.0003	0.1617 ± 0.0015	0.4192 ± 0.0035	14.5937 ± 0.0706	0.5470 ± 0.0667
	MCCA	0.1176 ± 0.0006	0.1612 ± 0.0017	0.4178 ± 0.0061	14.5641 ± 0.0847	0.5483 ± 0.0847
	OM ² CCA	0.1181 ± 0.0005	0.1626 ± 0.0016	0.4202 ± 0.0052	14.6236 ± 0.0982	0.5482 ± 0.1014
	HSIC-GEV	0.1131 ± 0.0008	0.1507 ± 0.0011	0.3460 ± 0.0024	13.9975 ± 0.0970	0.5868 ± 0.1280
OHSIC	0.1169 ± 0.0003	0.1586 ± 0.0014	0.4127 ± 0.0058	14.4238 ± 0.0572	0.5530 ± 0.0572	
pascal07	view-1	0.0730 ± 0.0005	0.2786 ± 0.0049	0.5946 ± 0.0029	6.9247 ± 0.1447	0.4425 ± 0.1447
	view-2	0.0729 ± 0.0002	0.2708 ± 0.0046	0.5950 ± 0.0031	6.7332 ± 0.1332	0.4466 ± 0.1332
	view-3	0.0715 ± 0.0005	0.2373 ± 0.0033	0.5819 ± 0.0044	5.9969 ± 0.1021	0.4800 ± 0.0754
	view-4	0.0702 ± 0.0003	0.2328 ± 0.0041	0.5656 ± 0.0042	5.8909 ± 0.0956	0.4928 ± 0.0956
	view-5	0.0716 ± 0.0004	0.2714 ± 0.0031	0.5941 ± 0.0026	6.7623 ± 0.0936	0.4482 ± 0.0936
	view-6	0.0719 ± 0.0006	0.2692 ± 0.0042	0.5945 ± 0.0022	6.7054 ± 0.0993	0.4498 ± 0.0993
	view-7	0.0699 ± 0.0005	0.2219 ± 0.0032	0.5617 ± 0.0049	5.6492 ± 0.0718	0.5006 ± 0.0718
	concat	0.0700 ± 0.0003	0.2268 ± 0.0045	0.5634 ± 0.0061	5.7465 ± 0.1130	0.4996 ± 0.1130
	MCCA	0.0691 ± 0.0002	0.2183 ± 0.0029	0.5700 ± 0.0054	5.5241 ± 0.0599	0.4991 ± 0.0599
	OM ² CCA	0.0694 ± 0.0003	0.2179 ± 0.0037	0.5723 ± 0.0060	5.5003 ± 0.0788	0.4960 ± 0.0714
	HSIC-GEV	0.0678 ± 0.0004	0.2185 ± 0.0052	0.5569 ± 0.0046	5.4652 ± 0.1018	0.5088 ± 0.1018
OHSIC	0.0678 ± 0.0004	0.2122 ± 0.0034	0.5604 ± 0.0046	5.3753 ± 0.0679	0.5073 ± 0.0525	

set of predefined categories, i.e., a subset of labels. In addition, the multi-view multi-label classification data consists of multiple views as the input. It is different from multi-view feature extraction in Section 6.1, where each instance only has a single label.

Following [12, 23], we first use a multi-view subspace learning method as a supervised dimensionality reduction step for the purpose multi-view multi-label classification so that the embeddings obtained by the method hopefully encode important correlations among multiple views and their output labels, and then multi-label classification is conducted in the common space. Hence, it is expected to have better performance for multi-view multi-label classification comparing with a single-view method applied to each view only or to the naive concatenation approach. Specifically, we compare the following multi-view subspace learning approaches:

- view- s : PCA on the s th view.
- concat: the concatenation of all views in the common space by PCA.
- MCCA [5]: the output labels considered as an additional view. Hence, there are $v + 1$ views. The projection matrix for the output labels is learned but not used.
- HSIC-GEV: the proposed model solved as a generalized eigenvalue problem, which is similar to MLDA, but $\Phi_{s,s}$ is defined in (30a) catering for multi-label outputs.
- OM²CCA: the proposed model instantiated from (23) for $v + 1$ views with (28). Different from [23], all multiple views as input are used.
- OHSIC: the proposed model instantiated from (23) with (30).

After the projection matrices are learned, we apply ML-kNN⁸ in the common space as the backend multi-label classifier [61], which has demonstrated good performance over various datasets.

6.2.3. Performance Evaluation. Five widely-used metrics are used to measure the performance, including Hamming Loss, One Error, Ranking Loss, Coverage and Average Precision. Each evaluates the performance of a multi-label predictor from different aspects. Their concrete definitions can be found in [62]. In particular, the larger the Average Precision is, the better the performance, while for the other four metrics, the smaller the value the better the performance. Following [61], for each method we report the best results and their standard deviations over 10 random training/testing splits in each of the five metrics.

Results by compared methods are shown in Table 4, in which the best results are reported by tuning $\alpha \in \{0.01, 0.1, 1, 10, 100\}$ and $k \in \{2, 5 : 5 : 50\}$ except for emotions, mirflickr and pascal07 (MCCA and OM²CCA cannot have k larger than the number of labels), over 10 random splits of 10% training and 90% testing. From Table 4, it can be observed that (i) the joint subspace learning methods generally work better than PCA and the concatenation of individually projected views by PCA, (ii) the proposed HSIC-GEV and OHSIC consistently outperform others except in terms of Ranking Loss on emotions, Corel5k and espgame, and (iii) HSIC-GEV takes the top spots on iaprtc12 and mirflickr, while OHSIC takes most of the top spots on emotions, Corel5k and espgame. On pascal07, both approaches work equally well.

We further investigate the impact of parameter k on each of the five metrics. Fig. 4 shows the trends of five metrics on Corel5k and pascal07 as k varies. It is observed that a large k generally leads to better performance for all methods, as it should be. Although Hamming Loss on Corel5k shows some fluctuation, the

⁸<http://lamda.nju.edu.cn/files/MLkNN.rar>

absolute difference is negligibly in the order of 10^{-5} . In summary, HSIC-GEV and OHSIC can work consistently well over all tested ks .

7. CONCLUSION

In this paper, we start by proposing a unified multi-view subspace learning framework, which aims to learn a set of orthogonal projections for desirable advantages such as more noise-tolerant, better suited for data visualization and distance preservation. The proposed framework can be easily extended for single-view and multi-view learning in the settings of both unsupervised and supervised learning. An efficient successive approximations via eigenvectors method (OSAVE) is designed to approximately solve the optimization problem resulted from the proposed framework. It is built upon well developed numerical linear algebra technique and can handle large scale datasets. To verify the capability of the proposed framework and the approximate optimization method, we showcases six new models for two learning tasks. Experimental results on various real-world datasets demonstrate that our proposed models solved by our successive approximation method OSAVE perform competitively to and often better than the baselines.

REFERENCES

- [1] Y. Peng and J. Qi, "CM-GANs: Cross-modal generative adversarial networks for common representation learning," *ACM Transactions on Multimedia Computing, Communications, and Applications (TOMM)*, vol. 15, no. 1, pp. 1–24, 2019.
- [2] J. Zhao, X. Xie, X. Xu, and S. Sun, "Multi-view learning overview: Recent progress and new challenges," *Information Fusion*, vol. 38, pp. 43–54, 2017.
- [3] C. Xu, D. Tao, and C. Xu, "A survey on multi-view learning," *arXiv preprint arXiv:1304.5634*, 2013.
- [4] H. Hotelling, "Relations between two sets of variates," *Biometrika*, vol. 28, no. 3-4, pp. 321–377, 1936.
- [5] A. A. Nielsen, "Multiset canonical correlations analysis and multispectral, truly multitemporal remote sensing data," *IEEE Transactions on Image Processing*, vol. 11, no. 3, pp. 293–305, 2002.
- [6] D. R. Hardoon, S. Szedmak, and J. Shawe-Taylor, "Canonical correlation analysis: An overview with application to learning methods," *Neural Computation*, vol. 16, no. 12, pp. 2639–2664, 2004.
- [7] G. Andrew, R. Arora, J. Bilmes, and K. Livescu, "Deep canonical correlation analysis," in *International Conference on Machine Learning*, 2013, pp. 1247–1255.
- [8] A. Sharma, A. Kumar, H. Daume, and D. W. Jacobs, "Generalized multiview analysis: A discriminative latent space," in *2012 IEEE Conference on Computer Vision and Pattern Recognition*. IEEE, 2012, pp. 2160–2167.
- [9] G. Cao, A. Iosifidis, K. Chen, and M. Gabbouj, "Generalized multi-view embedding for visual recognition and cross-modal retrieval," *IEEE Transactions on Cybernetics*, vol. 48, no. 9, pp. 2542–2555, 2018.
- [10] S. Sun, X. Xie, and M. Yang, "Multiview uncorrelated discriminant analysis," *IEEE Transactions on Cybernetics*, vol. 46, no. 12, pp. 3272–3284, 2015.
- [11] L. Sun, S. Ji, and J. Ye, "Canonical correlation analysis for multilabel classification: A least-squares formulation, extensions, and analysis," *IEEE Transactions on Pattern Analysis and Machine Intelligence*, vol. 33, no. 1, pp. 194–200, 2010.
- [12] L. Wang, L.-H. Zhang, Z. Bai, and R.-C. Li, "Orthogonal canonical correlation analysis and applications," *Optimization Methods and Software*, pp. 1–21, 2020.
- [13] I. T. Jolliffe, "Principal components in regression analysis," in *Principal Component Analysis*. Springer, 1986, pp. 129–155.
- [14] J. Ye, "Characterization of a family of algorithms for generalized discriminant analysis on undersampled problems," *Journal of Machine Learning Research*, vol. 6, no. Apr, pp. 483–502, 2005.

- [15] H. Wang, S. Yan, D. Xu, X. Tang, and T. Huang, "Trace ratio vs. ratio trace for dimensionality reduction," in *2007 IEEE Conference on Computer Vision and Pattern Recognition*. IEEE, 2007, pp. 1–8.
- [16] L.-H. Zhang, L.-Z. Liao, and M. K. Ng, "Fast algorithms for the generalized Foley-Sammon discriminant analysis," *SIAM J. Matrix Anal. Appl.*, vol. 31, no. 4, pp. 1584–1605, 2010.
- [17] E. Kokiopoulou and Y. Saad, "Orthogonal neighborhood preserving projections: A projection-based dimensionality reduction technique," *IEEE Transactions on Pattern Analysis and Machine Intelligence*, vol. 29, no. 12, pp. 2143–2156, 2007.
- [18] D. Cai and X. He, "Orthogonal locality preserving indexing," in *Proceedings of the 28th annual international ACM SIGIR Conference on Research and Development in Information Retrieval*. ACM, 2005, pp. 3–10.
- [19] K. Q. Weinberger, F. Sha, and L. K. Saul, "Learning a kernel matrix for nonlinear dimensionality reduction," in *Proceedings of the Twenty-first International Conference on Machine Learning*, 2004, p. 106.
- [20] L. Wang, Q. Mao, and I. W. Tsang, "Latent smooth skeleton embedding," in *Thirty-First AAAI Conference on Artificial Intelligence*, 2017.
- [21] X. Shen, Q. Sun, and Y. Yuan, "Orthogonal canonical correlation analysis and its application in feature fusion," in *Proceedings of the 16th International Conference on Information Fusion*, 2013, pp. 151–157.
- [22] J. P. Cunningham and Z. Ghahramani, "Linear dimensionality reduction: Survey, insights, and generalizations," *J. Mach. Learning Res.*, vol. 16, pp. 2859–2900, 2015.
- [23] L. Zhang, L. Wang, Z. Bai, and R.-C. Li, "A self-consistent-field iteration for orthogonal cca," *IEEE Transactions on Pattern Analysis and Machine Intelligence*, 2020, to appear.
- [24] X. Shen and Q. Sun, "Orthogonal multiset canonical correlation analysis based on fractional-order and its application in multiple feature extraction and recognition," *Neural Processing Letters*, vol. 42, no. 2, pp. 301–316, 2015.
- [25] L. Wang and R.-C. Li, "A scalable algorithm for large-scale unsupervised multi-view partial least squares," *IEEE Transactions on Big Data*, 2020, to appear.
- [26] P. Hu, D. Peng, Y. Sang, and Y. Xiang, "Multi-view linear discriminant analysis network," *IEEE Transactions on Image Processing*, vol. 28, no. 11, pp. 5352–5365, 2019.
- [27] X. He, D. Cai, and P. Niyogi, "Laplacian score for feature selection," in *Advances in Neural Information Processing Systems*, 2006, pp. 507–514.
- [28] M. Sugiyama, "Dimensionality reduction of multimodal labeled data by local fisher discriminant analysis," *Journal of Machine Learning Research*, vol. 8, no. May, pp. 1027–1061, 2007.
- [29] F. Nie, S. Xiang, Y. Jia, and C. Zhang, "Semi-supervised orthogonal discriminant analysis via label propagation," *Pattern Recognition*, vol. 42, no. 11, pp. 2615–2627, 2009.
- [30] L.-H. Zhang, "Uncorrelated trace ratio LDA for undersampled problems," *Patt. Recog. Lett.*, vol. 32, pp. 476–484, 2011.
- [31] S. Yan, D. Xu, B. Zhang, H.-J. Zhang, Q. Yang, and S. Lin, "Graph embedding and extensions: A general framework for dimensionality reduction," *IEEE Transactions on Pattern Analysis and Machine Intelligence*, vol. 29, no. 1, pp. 40–51, 2006.
- [32] X. He and P. Niyogi, "Locality preserving projections," in *Advances in Neural Information Processing Systems*, 2004, pp. 153–160.
- [33] M. Belkin and P. Niyogi, "Laplacian eigenmaps and spectral techniques for embedding and clustering," in *Advances in Neural Information Processing Systems*, 2002, pp. 585–591.
- [34] S. T. Roweis and L. K. Saul, "Nonlinear dimensionality reduction by locally linear embedding," *Science*, vol. 290, no. 5500, pp. 2323–2326, 2000.
- [35] J. B. Tenenbaum, V. De Silva, and J. C. Langford, "A global geometric framework for nonlinear dimensionality reduction," *Science*, vol. 290, no. 5500, pp. 2319–2323, 2000.
- [36] Z. Bai, J. Demmel, J. Dongarra, A. Ruhe, and H. van der Vorst (editors), *Templates for the solution of Algebraic Eigenvalue Problems: A Practical Guide*. Philadelphia: SIAM, 2000.
- [37] G. H. Golub and C. F. Van Loan, *Matrix Computations*, 4th ed. Baltimore, Maryland: Johns Hopkins University Press, 2013.
- [38] P.-A. Absil, R. Mahony, and R. Sepulchre, *Optimization Algorithms On Matrix Manifolds*. Princeton University Press, 2008.
- [39] J. Nocedal and S. Wright, *Numerical Optimization*, 2nd ed. Springer, 2006.
- [40] Z. Wen and W. Yin, "A feasible method for optimization with orthogonality constraints," *Math. Program.*, vol. 142, no. 1-2, pp. 397–434, 2013.

- [41] A. Gretton, O. Bousquet, A. Smola, and B. Schölkopf, “Measuring statistical dependence with hilbert-schmidt norms,” in *International Conference on Algorithmic Learning Theory*. Springer, 2005, pp. 63–77.
- [42] R.-C. Li, “Rayleigh quotient based optimization methods for eigenvalue problems,” in *Matrix Functions and Matrix Equations*, ser. Series in Contemporary Applied Mathematics, Z. Bai, W. Gao, and Y. Su, Eds. Singapore: World Scientific, 2015, vol. 19, pp. 76–108, lecture summary for 2013 Gene Golub SIAM Summer School.
- [43] A. V. Knyazev, “Toward the optimal preconditioned eigensolver: Locally optimal block preconditioned conjugate gradient method,” *SIAM J. Sci. Comput.*, vol. 23, no. 2, pp. 517–541, 2001.
- [44] G. Golub and Q. Ye, “An inverse free preconditioned Krylov subspace methods for symmetric eigenvalue problems,” *SIAM J. Sci. Comput.*, vol. 24, pp. 312–334, 2002.
- [45] J. Demmel, *Applied Numerical Linear Algebra*. Philadelphia, PA: SIAM, 1997.
- [46] M. T. Chu and J. L. Watterson, “On a multivariate eigenvalue problem, part I: Algebraic theory and a power method,” *SIAM J. Sci. Comput.*, vol. 14, no. 5, pp. 1089–1106, 1993.
- [47] L.-H. Zhang, “Riemannian Newton method for the multivariate eigenvalue problem,” *SIAM J. Matrix Anal. Appl.*, vol. 31, no. 5, pp. 2972–2996, 2010.
- [48] —, “Riemannian trust-region method for the maximal correlation problem,” *Numer. Funct. Anal. Optim.*, vol. 33, no. 3, pp. 338–362, 2012.
- [49] J. Wu and J. M. Rehg, “Where am i: Place instance and category recognition using spatial pact,” in *2008 Ieee Conference on Computer Vision and Pattern Recognition*. IEEE, 2008, pp. 1–8.
- [50] A. Oliva and A. Torralba, “Modeling the shape of the scene: A holistic representation of the spatial envelope,” *International Journal of Computer Vision*, vol. 42, no. 3, pp. 145–175, 2001.
- [51] T. Ojala, M. Pietikäinen, and T. Mäenpää, “Multiresolution gray-scale and rotation invariant texture classification with local binary patterns,” *IEEE Transactions on Pattern Analysis & Machine Intelligence*, no. 7, pp. 971–987, 2002.
- [52] S. Lazebnik, C. Schmid, and J. Ponce, “Beyond bags of features: Spatial pyramid matching for recognizing natural scene categories,” in *2006 IEEE Computer Society Conference on Computer Vision and Pattern Recognition (CVPR’06)*, vol. 2. IEEE, 2006, pp. 2169–2178.
- [53] F.-F. Li, R. Fergus, and P. Perona, “Learning generative visual models from few training examples: An incremental bayesian approach tested on 101 object categories,” *Computer Vision and Image Understanding*, vol. 106, no. 1, pp. 59–70, 2007.
- [54] P. Duygulu, K. Barnard, J. F. de Freitas, and D. A. Forsyth, “Object recognition as machine translation: Learning a lexicon for a fixed image vocabulary,” in *European Conference on Computer Vision*. Springer, 2002, pp. 97–112.
- [55] A. Makadia, V. Pavlovic, and S. Kumar, “A new baseline for image annotation,” in *European Conference on Computer Vision*. Springer, 2008, pp. 316–329.
- [56] M. Everingham, L. Van Gool, C. K. Williams, J. Winn, and A. Zisserman, “The pascal visual object classes (voc) challenge,” *International journal of computer vision*, vol. 88, no. 2, pp. 303–338, 2010.
- [57] M. J. Huiskes and M. S. Lew, “The mir flickr retrieval evaluation,” in *Proceedings of the 1st ACM International Conference on Multimedia Information Retrieval*, 2008, pp. 39–43.
- [58] M. Guillaumin, T. Mensink, J. Verbeek, and C. Schmid, “Tagprop: Discriminative metric learning in nearest neighbor models for image auto-annotation,” in *2009 IEEE 12th International Conference on Computer Vision*. IEEE, 2009, pp. 309–316.
- [59] M. Guillaumin, J. Verbeek, and C. Schmid, “Multimodal semi-supervised learning for image classification,” in *2010 IEEE Computer Society Conference on Computer Vision and Pattern Recognition*. IEEE, 2010, pp. 902–909.
- [60] G. Tsoumakas and I. Katakis, “Multi-label classification: An overview,” *International Journal of Data Warehousing and Mining (IJDWM)*, vol. 3, no. 3, pp. 1–13, 2007.
- [61] M.-L. Zhang and Z.-H. Zhou, “MI-knn: A lazy learning approach to multi-label learning,” *Pattern Recognition*, vol. 40, no. 7, pp. 2038–2048, 2007.
- [62] —, “A review on multi-label learning algorithms,” *IEEE Transactions on Knowledge and Data Engineering*, vol. 26, no. 8, pp. 1819–1837, 2013.